Molecular simulation of nonfacilitated membrane permeation

Ernest Awoonor-Williams, Christopher N. Rowley

Department of Chemistry, Memorial University of Newfoundland, St. John's, NL A1B 3X7 Canada

Abstract

This is a review. Non-electrolytic compounds typically cross cell membranes by passive diffusion. The rate of permeation is dependent on the chemical properties of the solute and the composition of the lipid bilayer membrane. Predicting the permeability coefficient of a solute is important in pharmaceutical chemistry and toxicology. Molecular simulation has proven to be a valuable tool for modeling permeation of solutes through a lipid bilayer. In particular, the solubility-diffusion model has allowed for the quantitative calculation of permeability coefficients. The underlying theory and computational methods used to calculate membrane permeability are reviewed. We also discuss applications of these methods to examine the permeability of solutes and the effect of membrane composition on permeability. The application of coarse grain and polarizable models is discussed.

Keywords: Review, Membrane, Lipid Bilayer, Permeation, Non-facilitated, Solubility-diffusion Model, Molecular Dynamics, Diffusion, PMF, Potential of Mean Force, Polarizable, Coarse Grain

Email address: crowley@mun.ca (Christopher N. Rowley)

1. Introduction

One function of a biological membrane is to serve as a barrier between the cytosol and extracellular environment (1; 2; 3). Intracellular compartments like mitochondria, the nucleus, etc, are also enclosed by membranes. The primary component of these membranes is amphiphilic lipids. These lipids consist of a polar or ionic headgroup and a tail that is comprised of one or more hydrocarbon chains. The hydrophilicity of the head groups and the hydrophobicity of the tails cause the lipids to spontaneously self-assemble into planar bilayers where the headgroups face the solution and the tails form a hydrophobic interior layer.

Solutes crossing the membrane must pass through the nonpolar lipid tail region of the membrane. Compounds that are more soluble in bulk water than they are in the nonpolar membrane interior will tend not to partition into the membrane. This simple mechanism allows these thin bilayers ($\sim 40-50$ Å thick) to provide an effective barrier for highly water-soluble compounds like ions and sugars. In pure lipid bilayers, the rates of permeation of these species are very low. In biological membranes, rapid permeation of these compounds can be facilitated by membrane proteins like channels or transporters (4; 5; 6).

Two distinct mechanisms have been proposed for permeation in the absence of a protein facilitator: passage through a transient water pore and direct permeation through the membrane (7). Rare fluctuations in the bilayer structure can form transient water pores that allow ionic compounds to cross the bilayer while still solvated by water. This avoids the high thermodynamic penalty for dehydrating the ion. The second mechanism applies to

non-electrolytic solutes, which can permeate directly through the membrane. This review will focus on molecular simulations of this second mechanism.

Many non-electrolytic compounds can permeate directly through the membrane because there is a significant probability for them to partition into the interior of the membrane. These compounds are generally only moderately soluble in aqueous solutions due to the lack of strong electrostatic interactions with water molecules. The London dispersion attractions between these solutes and the lipid tails can be competitive to their interactions with water, so the thermodynamic penalty for these compounds to enter the interior of the membrane is attenuated or even eliminated. To varying degrees, these compounds can undergo direct permeation without facilitation by a transmembrane protein.

The rate of permeation of a solute across a membrane is defined by its flux (J), which gives the number of molecules that cross a unit area of the membrane per unit time (e.g., μmol/s/cm^2). The flux is the product of the concentration gradient of the solute across the membrane (ΔC) and the permeability coefficient (P_m),

$$J = P_m \cdot \Delta C. \tag{1}$$

P_m depends on the type of permeating solute, the membrane composition, and the conditions that permeation occurs under (e.g., temperature). It has units of distance per unit time and is commonly reported in cm/s. For a constant set of conditions and membrane composition, the permeability coefficient provides a measure of the intrinsic membrane permeability of a solute. P_m is therefore the standard experimental and computational measure of the

permeability of a solute.

1.1. Experimental determination of permeability

A variety of experimental techniques are used to determine permeability coefficients. One of the most general techniques uses a planar bilayer separating two cells. A concentration gradient is created between the two cells and the change in concentration is measured after a time interval. Several techniques have been used to measure the solution concentrations, including radiolabeling (8), UV-Vis spectroscopy (9), and LC-MS (10).

The concentration of electrochemically-active species can be measured by selective microelectrodes near the surface of the membrane. In some cases, the electrode measures the permeating species directly (e.g., the permeation of K^+ (11)). Weak acids and bases typically permeate in their neutral, conjugate form, but their permeation can be measured by microelectrodes that detect the ionic forms that are formed in the solution at the surface of the membrane. For example, the permeability of ammonia has been measured by ammonium -selective electrodes (12). Similarly, the permeation of many weak acids has been measured by pH-sensitive microelectrodes that detect the small changes in pH at the surface of the membrane (13; 14). H_2O_2 permeability has been determined by an O_2-selective electrode by measuring concentrations of O_2 formed by the reduction of H_2O_2 inside the cell (15; 16).

Magnetic resonance techniques can be used to study the permeability of certain solutes. Electron paramagnetic resonance (EPR) can be used to measure the permeability of solutes with unpaired electrons, such as NO (17; 18; 19) and O_2 (20; 21). This technique is particularly powerful because the rate of diffusion at different depths within the membrane can be mea-

sured. ^{1}H and ^{17}O Nuclear Magnetic Resonance (NMR) has also been used to measure the rate of water permeation. Water molecules that permeate into a liposome containing paramagnetic metal complexes (e.g., Mn(II), Ln(III), or Gd(III)) will undergo a rapid spin relaxation, allowing the rate at which water molecules cross the membrane to be determined (22).

Fluorescence spectroscopy can be used to measure the permeability of solutes that affect fluorophores loaded inside liposomes. The transmembrane permeation of protons was measured by the change in fluorescence of pyranine, a pH-sensitive dye (11). Water permeability has been calculated from the increase in self-quenching of carboxyfluorescein as the volume of the liposome decreases in response to osmotic pressure (23). The permeation of the fluorophore itself can also be measured if the fluorescence is affected by the contents of the liposome. For example, the permeation of tetracyclines was measured by the observation of the enhanced fluorescence of a Tet-repressor-bound tetracycline inside a liposome (24). The rate of permeation of aromatic-containing acids, like salicylic acid, into liposomes has been measured by monitoring the fluorescence of Tb^{3+}-carboxylate complexes (25).

One limitation to permeability measurements using liposomes is that stopped-flow devices are often used to create the concentration gradient between the solution and the interior of the liposome. Pohl and coworkers noted that the mixing time associated with this technique means that they cannot be used to study very fast rates of permeation and are restricted to solutes where $P_m < 10^{-2}$ cm/s (26).

These techniques have a range of capabilities and limitations. Simple

planar-bilayer cells can be used across a range of solutes, provided that permeation is slower than the solution mixing time. Liposomes loaded with fluorescent reporters can also be used with slowly-permeating solutes that can be measured by fluorescence spectroscopy. Microelectrode methods can be used when the concentration of the solute can be measured electrochemically or can be measured indirectly by a change in an equilibrium (e.g., pH), although this can involve complicated kinetic models due to multi-species equilibria and unstirred layers at the membrane-water interface (27; 13; 28). Magnetic resonance methods, like EPR and NMR, can only be used for select solutes. The challenges associated with experimental permeability measurements have encouraged the development of molecular simulation methods that can support experimental results and provide insight into trends in permeability.

1.2. Permeability Models

Understanding the relationship between the chemical properties of the solute and its permeability is important for predicting the toxicity and pharmacokinetics of a compound (29; 30; 31). Models for predicting membrane permeability date back well over 100 years; publications by Meyer in 1899 and Overton in 1901 established the relationship between high rates of nonfacilitated membrane permeation and the hydrophobicity of the solute (32; 33). Walter and Gutknecht quantified this observation by showing that there is strong linear correlation between the log of the permeability coefficient and the log of water-alkane partition coefficients for a wide range of neutral solutes (34). This supports the Meyer–Overton rule that the rate of permeation is proportional to the relative solubility of the solute in the apolar membrane

interior vs an aqueous solution.

Several experimental and theoretical models have been developed to predict permeability (35; 36; 37; 29; 30), with varying degrees of success, but the advent of computer simulations have led to the most significant developments. Molecular simulation methods for lipid bilayers have made it possible to study the permeation of solutes without direct empirical inputs. These simulations have provided atomic-scale interpretations of these data and quantitative interpretations of permeability trends in terms of the solution thermodynamics and dynamics. Empirically-based principles of permeation like the Meyer–Overton rule can now be interpreted within a rigorous physical framework. This review presents some of the research on the simulation of nonfacilitated permeation over the last 20 years. Interested readers may also be interested in a recent review by MacCallum and Tieleman on simulations of small molecules interacting with lipid bilayers (38) and a review by Orsi and Essex on modeling permeability (39).

2. Development of the solubility-diffusion model

To develop a quantitative theory for nonfacilitated permeation, the membrane is described as a fluid environment that the permeant passes through by Brownian motion. This model is consistent with direct molecular dynamics simulations of membrane permeation. Fig. 1 shows the trajectory of a O_2 molecule permeating through a DPPC bilayer. The solute undergoes an effectively random walk along the z-axis before exiting the opposite side of the membrane. The solute also undergoes significant lateral motion inside the bilayer in the xy plane, but a rate theory can be developed based on the

net flux (J) of the solute along the z-axis alone.

The dynamics of the solute are complicated by the inhomogeneity of the bilayer, which varies in chemical composition and density along the transmembrane axis, z. In the inhomogenous solubility-diffusion model model, both the solute diffusivity ($D(z)$) and potential of mean force (PMF, $w(z)$) vary as a function of the position of the solute along the z axis. $w(z)$ is related to the solubility of the solute at z, $K(z) = \exp(-w(z)/k_BT)$, so this model is commonly referred to as the solubility-diffusion model.

The one-dimensional Nernst–Planck equation for a neutral solute in an inhomogeneous medium (40; 41) provides an expression for the flux through a unit area of the membrane at depth z ($J(z)$),

$$J(z) = -D(z)\frac{\mathrm{d}C(z)}{\mathrm{d}z} - C(z)D(z)\frac{\mathrm{d}\left(w(z)/k_BT\right)}{\mathrm{d}z}, \tag{2}$$

where $C(z)$ is the concentration of the solute.

Multiplying both sides of the equation by $e^{w(z)/k_BT}/D(z)$ gives,

$$\frac{J(z)e^{w(z)/k_BT}}{D(z)} = -e^{w(z)/k_BT}\frac{\mathrm{d}C(z)}{\mathrm{d}z} - e^{w(z)/k_BT}C(z)\frac{\mathrm{d}\left(w(z)/k_BT\right)}{\mathrm{d}z} \tag{3}$$

The right hand side of this equation can be combined into a single differential,

$$\frac{J(z)e^{w(z)/k_BT}}{D(z)} = -\frac{\mathrm{d}}{\mathrm{d}z}\left(C(z)e^{w(z)/k_BT}\right) \tag{4}$$

To determine the flux across the entire bilayer, this equation is integrated with respect to z over the interval $[-L/2, L/2]$ where L is the width of a bilayer centered at $z = 0$,

$$\int_{-L/2}^{L/2}\frac{J(z)e^{w(z)/k_BT}}{D(z)}\mathrm{d}z = -\int_{-L/2}^{L/2}\frac{\mathrm{d}}{\mathrm{d}z}\left(C(z)e^{w(z)/k_BT}\right)\mathrm{d}z \tag{5}$$

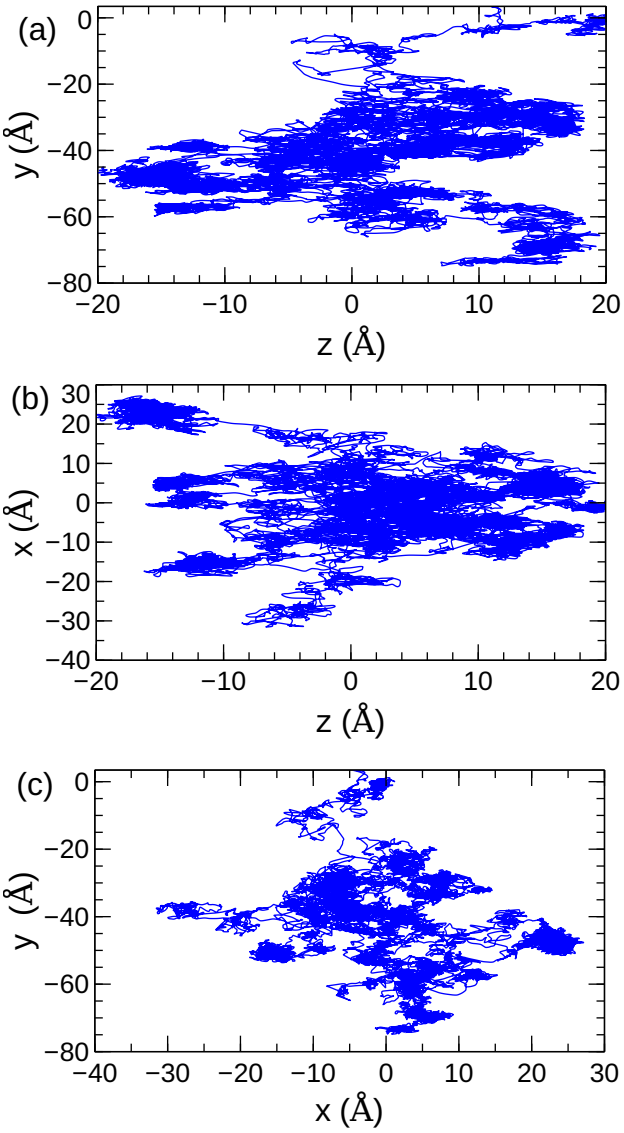

Figure 1: 2D representations of a 300 ps trajectory of an O_2 molecule permeating from the lower interface ($z = -20$ Å) to the upper interface ($z = 20$ Å) of a DPPC bilayer. The z axis corresponds to permeation across the bilayer, while the x and y axes are in the plane of the bilayer–water interface. The trajectory plotted in (a) and (b) show permeation consistent with Brownian motion, with the solute moving back and forth along the z axis before reaching the opposite interface. Plot (c) shows that there is significant lateral diffusion of the solute in the xy-plane during permeation.

Under steady-state conditions, the flux at any value of z will be constant, so J can be factored out of the integral. Through rearrangement and simplification, the equation becomes,

$$J \int_{-L/2}^{L/2} \frac{e^{w(z)/k_BT}}{D(z)} \mathrm{d}z = -\left[C(z)e^{w(z)/k_BT}\right]_{-L/2}^{L/2} \tag{6}$$

Isolating J on the left hand side and evaluating the bounds on the integral on the right hand side gives,

$$J = -\frac{1}{\int_{-L/2}^{L/2} \frac{e^{w(z)/k_BT}}{D(z)} \mathrm{d}z} \left[C(L/2)e^{w(L/2)/k_BT} - C(-L/2)e^{w(-L/2)/k_BT}\right] \tag{7}$$

By definition, $w(z)$ is zero in the solution outside the bilayer, so $w(L/2) = w(-L/2) = 0$. This gives the final form of the equation for the flux,

$$J = -\frac{1}{\int_{-L/2}^{L/2} \frac{e^{w(z)/k_BT}}{D(z)} \mathrm{d}z} \left[C(L/2) - C(-L/2)\right]. \tag{8}$$

$C(-L/2) - C(L/2)$ is the concentration difference across the bilayer in the direction of the positive flux, ΔC. By comparison to Eqn. 1, the permeability coefficient is,

$$\frac{1}{P_m} = \int_{-L/2}^{L/2} \frac{e^{w(z)/k_BT}}{D(z)} \mathrm{d}z \tag{9}$$

Alternative derivations are available in Diamond and Katz (42) and Marrink and Berendsen (43; 44). An elaboration that includes the orientational degrees of freedom of the solute is presented in Ref. 45.

Several assumptions are made in this derivation. The flux is assumed to be under steady state conditions with a negligible concentration gradient across the membrane. The membrane must be sufficiently laterally homogeneous so that meaningful averages of $w(z)$ and $D(z)$ can be determined. For

example, a permeability rate that is governed by the formation of a water-pore that allows passage of the solute would not be well described by this model (7; 46). The solute dynamics are described by Brownian motion, which is only valid for individual solute molecules moving through high-friction environments on a reasonably flat free energy surface. The permeation of a solute with a variable number of associated water molecules would also be affected by the rates of hydration/dehydration inside the membrane and is not entirely consistent with this model.

To calculate P_m using this theory, $D(z)$ and $w(z)$ must be determined for the full width of the membrane. These data can then be used to evaluate the integral in Eqn. 9 numerically. The bounds of the integration are also ambiguous because the membrane interface is diffuse; $w(z)$ and $D(z)$ must be calculated over a broad range so that the bounds on the integral can be determined based on when these values plateau to their bulk solution values. The practical aspects of calculating these profiles are presented in the following sections.

3. Practical aspects

3.1. Simulation systems

Simulations of membrane permeability are typically performed with periodic unit cells. A planar bilayer is constructed in the cell to form a lamellar system. Water layers are added above and below the bilayer. By convention, the bilayer interface extends along the xy plane and the z-axis corresponds to the transmembrane axis (a.k.a., the bilayer normal). Recent simulations commonly include 60–200 lipids (47; 48; 49). The water layers must be sufficiently

thick so that periodic membrane–membrane interactions are minimized and so $D(z)$ and $w(z)$ can be calculated at distances that are sufficiently far from the water-lipid interface to establish a reference (i.e., $w(z_{\text{bulk}}) = 0$). Studies have used simulation cells with various sizes, but bilayer surface areas in the $(40 - 60)^2$ Å^2 range and cell heights of 80 – 110 Å in the z dimension are common. A typical simulation cell is shown in Fig. 2.

A wide range of force fields have been used in recent permeation simulations. The TIP3P (50) and TIP4P (51) water models are both popular. The Berger (52) and CHARMM36 (53) lipid models have both been used successfully. The permeating solutes have been described using specific force fields or generalized force fields like GAFF (54), OPLS (55), or CGenFF (56). Polarizable and coarse grain models are also available. These are discussed in Sections 5.1 and 5.2.

3.2. Calculation of the Potential of Mean Force

The potential of mean force of the permeation of the solute along the z-axis ($w(z)$) can be calculated using a range of free energy methods. The first PMFs calculated by Marrink and Berendsen used (43),

$$w(z) = -\int_{-L}^{z} \langle F_z(z') \rangle_{z'} \mathrm{d}z' \tag{10}$$

where $F_z(z')$ is the force on the solute along the z-axis when the solute is constrained at z'.

To sample the ensemble average of $F_z(z')$, ($\langle F_z \rangle_{z'}$), the equations of motion must be modified so that the solute is constrained to a value of z'. The z-component of the force on the solute by the environment are averaged over

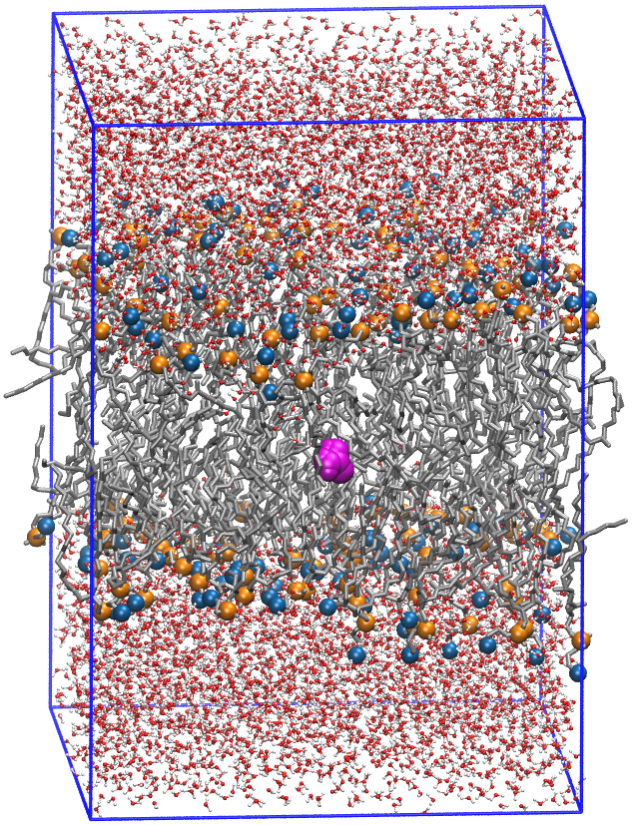

Figure 2: An example simulation cell used to simulate membrane permeation. A bilayer section with a 62 Å × 62 Å surface area and containing 128 1,2-dimyristoyl-sn-glycero-3-phosphocholine (DMPC) lipids is oriented in the xy plane of the cell. Lipid tails are rendered in gray. Lipid heads are rendered in blue (choline) and orange (phosphate). The bilayer is surrounded by water layers (red and white). A permeating molecule of urea is at the center of the bilayer (magenta).

long MD simulations at a series of positions spanning the membrane. The integral is numerically integrated to yield $w(z)$.

Most recent permeability simulations use umbrella sampling to calculate $w(z)$ (57; 58). In this method, a series of simulations are performed with the solute restrained relative to the center of mass of the membrane using a harmonic potential,

$$u_i(z) = \frac{1}{2}k(z - z_{0,i})^2, \tag{11}$$

where $u_i(z)$ is the potential energy of the restraint for simulation i, k is the force constant of the restraint, and $z_{0,i}$ is the reference position along the z axis the simulation is biased to sample near.

These simulations are performed with values of $z_{0,i}$ separated by regular intervals, such that a solute is simulated extensively at every point spanning the membrane. The optimal choices of window spacing and force constant (k) depends on the membrane composition, temperature, and solute. Recent studies have used window spacings that vary between 0.2 and 1.0 Å separations and force constants in the $k = 1.2-7.2$ kJ mol^{-1} Å^{-2} range (59; 48; 47). In systems where the PMF varies sharply with z, sections of the PMF may require more extensive sampling (60), so additional windows at smaller spacings and stronger force constants can be added in these regions (59). $G(z)$ can be constructed from the distributions sampled in these simulations using techniques like Weighted Histogram Analysis Method (WHAM) (61; 62; 63) or the multistate Bennett acceptance ratio estimator (MBAR) (63).

Neale et al. showed that umbrella sampling simulations for the partitioning of arginine and isoleucine side chain models into a bilayer required very extensive simulations to achieve sub-kcal convergence (60). This was

particularly serious for the charged arginine group, which required a 125 ns equilibration and μs length sampling per umbrella sampling window to eliminate systematic errors. This was attributed to distortions in the bilayer that occur over long timescales. Even the calculation of permeation PMFs of small nonpolar solutes requires equilibration simulations that are several nanoseconds long and a sampling period greater than 10 ns. Performing several independent simulations from different initial configurations can help identify if the PMF has reached convergence.

The slow convergence of permeation umbrella sampling simulations can be addressed by enhanced sampling techniques. Hamiltonian-exchange molecular dynamics allows neighboring windows of an umbrella sampling simulation to periodically exchange coordinates (64; 58). This can be applied to the calculation of membrane permeation PMFs by allowing exchanges of neighboring umbrella sampling windows along the z axis. For example, exchanges are periodically attempted between the simulation where $z_0 = 4$ Å and the simulation where $z_0 = 5$ Å. Neale et al. (47) developed a Hamiltonian exchange method for membrane permeation PMFs based on the virtual replica exchange method of Rauscher et al. (65). This method was found to have 300% better sampling efficiency than conventional umbrella sampling simulations.

Huang and Garcia applied the Replica Exchange with Solute Tempering (REST) enhanced sampling method to the simulation of lipid bilayers (66). In this technique, the simulation of the bilayer is allowed to undergo exchanges with simulations where the solute and bilayer are coupled to different thermostats and lipid-lipid interactions are biased. This allows rapid

lateral diffusion of the lipids and could improve the sampling of the configurational space of the permeating solutes. Jaäbeck and Lyubartsev have found that metadynamics can help sample solute conformational degrees of freedom, which allows better sampling of the PMF of permeation (67).

The permeation of large amphiphilic solutes is complicated by the dynamics of secondary degrees of freedom. Even for small amphiphiles, like alcohols, the solute must undergo a "flip-flop" transition, where the hydrophilic head reorients to be directed towards the opposing membrane interface when it passes through the bilayer interior. The transitions between these orientations can require time scales greater than nanoseconds, so a conventional umbrella sampling simulation along the z axis may not provide an accurate description of the permeation.

This sampling issue with amphiphilic solutes can be addressed by biasing the simulation to sample the orientational degrees of freedom of the solute. Jo et al. calculated the PMF for the transition of cholesterol from one bilayer leaflet to the other by a 2D umbrella sampling simulation of position of center of mass along the z-axis and the tilt angle of the solute with respect to the plane of the bilayer (68). Comer et al. developed a method that incorporates the dynamics of the solute along z and its orientation with respect to the xy plane of the membrane (69). Similarly, Parisio et al. developed an extension to the solubility-diffusion model where the rotation of the solute is explicitly included (45). Based on this model, Pariso, Sperotto, and Ferrarini concluded that the predominant pathway involved reorientation of the steroid while in the top leaflet so that its headgroup points towards the opposite side of the bilayer, then permeation along the z axis to enter the lower leaflet (70).

3.3. Calculation of the diffusivity profile

The solubility-diffusion model requires the calculation of the diffusion coefficient of the solute as a function of the position of the solute along the z-axis ($D(z)$). The Einstein equation allows the diffusion of the solute to be calculated by performing an MD simulation and calculating the mean square displacement of the solute along the z-axis (71),

$$D_z = \frac{1}{2Dt}\langle |z(t) - z(0)|^2 \rangle. \tag{12}$$

Alternatively, the Green–Kubo relation allows diffusion coefficients to be calculated from the integral of the velocity autocorrelation function (72),

$$D_z = \int_0^\infty \langle v_z(0) \cdot v_z(t) \rangle \mathrm{d}t \tag{13}$$

The inhomogeneity of a lipid bilayer makes it difficult to apply these methods to the calculation of $D(z)$. These methods are not appropriate for calculating $D(z)$ because they assume the solution is homogeneous, so they cannot capture the variation of D with the position of the solute along z.

Hummer developed a method to calculate position-dependent diffusion coefficients by sampling the frequency of transitions between positions along a coordinate in an equilibrium MD simulation (73). The variation of solubility of the solute in the bilayer is a challenge for this method. If the solubility of the solute is low at any point of the profile (i.e., $w(z)$ is large), transitions across this part of the profile in an equilibrium MD simulation will be rare. Very extensive MD simulations would be needed to directly sample diffusion across the full bilayer except for the most permeable solutes.

One direct method of calculating $D(z)$ uses a relation from fluctuation–dissipation theory to calculate $D(z)$ using the autocorrelation function (ACF)

of the force on the solute when it is constrained at position z along the axis (72),

$$D(z') = \frac{(RT)^2}{\int_0^\infty \langle \delta F_z(z',0)\delta F_z(z',t)\rangle \mathrm{d}t} \tag{14}$$

Here, $\delta F_z(z',t)$ is the deviation of the force on the solute along the z axis at position z' from the average force ($\delta F_z(z,t) = F_z(z,t) - \langle F_z(z')\rangle$).

In practice, these calculations make use of the same type of simulations that can be used to calculate the PMF from the integral of the average force (Eqn. 10). The drawback of this method is that most MD codes would have to be modified in order to do these calculations. The equations of motion of the MD integration algorithm must be modified to constrain the solute to a particular value of z (74). Most standard simulation codes must also be modified to output the time series of the force on a single molecule.

Alternative techniques for calculating $D(z)$ are provided by solutions to the Generalized Langevin Equation (GLE) for a harmonic oscillator. Consider a simulation where the permeant is restrained at some value of z along the transmembrane axis using a harmonic potential (i.e., Eqn. 11). The motion of the solute can be modeled as a harmonic oscillator where the rest of the system serves at its frictional bath. The GLE expression for the dynamics of this oscillator is,

$$m\ddot{z} = -k(z - z_{0,i}) - m\int_0^t \dot{z}(\tau)M(t-\tau)\mathrm{d}\tau + R(t) \tag{15}$$

where $R(t)$ is the random force that originates from the degrees of freedom orthogonal to z. $M(t)$ is the memory kernel, which reflects the frictional forces on the solute. Beginning from this equation, Woolf and Roux derived

an expression for the diffusion coefficient at $\langle z \rangle_i$ in terms of the Laplace transform of the velocity ACF ($\hat{C}(s; z_i)$) (75; 76; 77).

$$D(z_i = \langle z \rangle_i) = \lim_{s \to 0} \frac{-\hat{C}(s; z_i) \langle \delta z^2 \rangle_i \langle \dot{z}^2 \rangle_i}{\hat{C}(s; z_i) \left[s \langle \delta z^2 \rangle_i + \langle \dot{z} \rangle_i / s \right] - \langle \delta z^2 \rangle_i \langle \dot{z}^2 \rangle_i} \tag{16}$$

Because this equation has a singularity at $s = 0$, the limit cannot be taken directly. Instead, the Laplace transform must be performed numerically for a series of values of s and then the value of $s = 0$ must be extrapolated from these points.

Hummer derived a simpler expression based on this theory that relates $D(z)$ to the variance of z and the correlation time (τ) (73),

$$D(z_i = \langle z \rangle_i) = \frac{\mathrm{var}(z)^2}{\tau}. \tag{17}$$

τ is calculated from the integral of the position ACF ($C_{zz}(t)$).

$$\tau = \int_0^\infty C_{zz}(t) \mathrm{d}t \tag{18}$$

C_{zz} can be calculated by direct summation of pairs over the time series (78),

$$C_{zz}(t) = \langle \delta z(0) \delta z(t) \rangle = \frac{1}{n_{\mathrm{samples}}} \sum_{i=0}^{n_{\mathrm{samples}}} \delta z(i) \delta z(t+i) \tag{19}$$

where $\delta z(t) = z(t) - \langle z \rangle$.

Zhu and Hummer presented a further simplification that avoids calculation of a correlation function (79). In this method, τ is calculated from the variance of the mean value ($\bar{z}$) and the interval of the time series data points (Δt),

$$\tau \approx \left[\frac{n \cdot \mathrm{var}(\bar{z})}{\mathrm{var}(z)} - 1 \right] \frac{\Delta t}{2}. \tag{20}$$

$\bar{z}$ can be calculated using the block averaging method of Flyvbjerg and Petersen (80). This provides perhaps the simplest method for calculating $D(z)$ from time series data, although the analysis of the time series to calculate $D(z)$ using any of these methods is small in comparison to the cost of performing the MD simulations to generate the time series.

A key advantage of these methods is that they only require that the solute be restrained at a point along z with a harmonic potential with a reference position relative to the center of mass of the bilayer. This type of restraint is simple to implement and is available in most molecular dynamics codes. The diffusivity profile of a solute can be calculated by performing a series of MD simulations where the solute is restrained to positions at regular intervals along the z axis (e.g., 1 Å apart). This procedure is directly analogous to the umbrella sampling simulations using harmonic restraints that are used to calculate $w(z)$. In principle, both properties could be calculated from the same simulations. A time-series of the z position of this solute is collected from each simulation, which is then used to calculate the ACF.

In practice, the calculation of $D(z)$ is highly sensitive to the equilibration of the system and the length of sampling. Multiple simulations that are several nanoseconds long are needed to calculate well-converged ACFs. The spring constants of the harmonic potential (k) can affect the results because the description of the system with the GLE is based on the system acting as a harmonic oscillator in a frictional bath. Deviations away from this harmonic-oscillator model due to the effect of a rough underlying free energy surface

can introduce biases. Hummer also showed that $D(z)$ varies with the length of the interval the ACF is integrated over (73). Lastly, irregularities in the bilayer structure and the formation of water clusters around the solute can lead to large variations in $D(z)$. Improved methods for calculating position-dependent diffusivity profiles are an active subject of investigation (81; 82).

4. The solubility-diffusion model in practice

4.1. Interpreting permeation profiles

4.1.1. Bilayer regions

The diffusion and PMF profiles calculated by Marrink and Berendsen illustrated how the bilayer environment varies with depth (43; 83). The bilayer was divided into four overlapping regions that have different structural and chemical interactions with solutes, so the solutes will diffuse at different rates and have different solubility in these regions. The center of the bilayer is used as the point of reference ($z = 0$). The given ranges of z are approximate values for the DPPC bilayer example used in this review.

- Region I: $|z| > 25$ Å. The bulk solution. This region is primarily liquid water, with a small component of lipid headgroups.
- Region II: 17 Å $< |z| < 25$ Å. The lipid headgroups. These are typically solvated by water molecules.
- Region III: 10 Å $< |z| < 17$ Å. The upper portions of the lipid tails, acyl groups, and lower portions of the head groups.
- Region IV: $|z| < 10$ Å. The interface of the lipid tails of the two opposing monolayers at the center of the bilayer

These regions will be used to describe sections of the potential of mean force and diffusivity profiles discussed in the following sections. Marrink and Berendsen compared the PMFs of O_2 and H_2O as the prototypical examples of hydrophobic and hydrophilic permeants, respectively (83). These calculations were reproduced here using current models and simulation lengths (Fig. 3). The technical details of these simulations are included in Appendix A.

4.1.2. Potential of Mean Force

The PMF, $w(z)$ (a.k.a., $\Delta G(z)$), is the reversible work needed to move the solute from solution to the position z on the transmembrane axis. The PMF corresponds to the relative solubility of the permeant in solution vs the membrane interior; a positive PMF indicates that the solute is less soluble at this point in the membrane than it is in bulk solution, while a negative PMF indicates that it is more soluble. A highly positive PMF inside the membrane results in a small permeability coefficient, consistent with a low probability of the solute partitioning inside the bilayer to this position.

Hydrophobic solutes like O_2 have a small increase in the PMF at the water-lipid interface. The PMF drops once the solute reaches the ester/tail regions (Regions III & IV). For many hydrophobic solutes, the PMF reaches a minimum at $z = 0$ Å, indicating that these hydrophobic compounds will concentrate at the center of the bilayer. The thermodynamic driving force for this effect was investigated by MacCallum et al. by decomposing the PMF of hexane permeation into enthalpy and entropy components (59). Although the PMF across the bilayer was broad and flat, with a minimum at the center, the entropy and enthalpy components of the PMF varied significantly as the

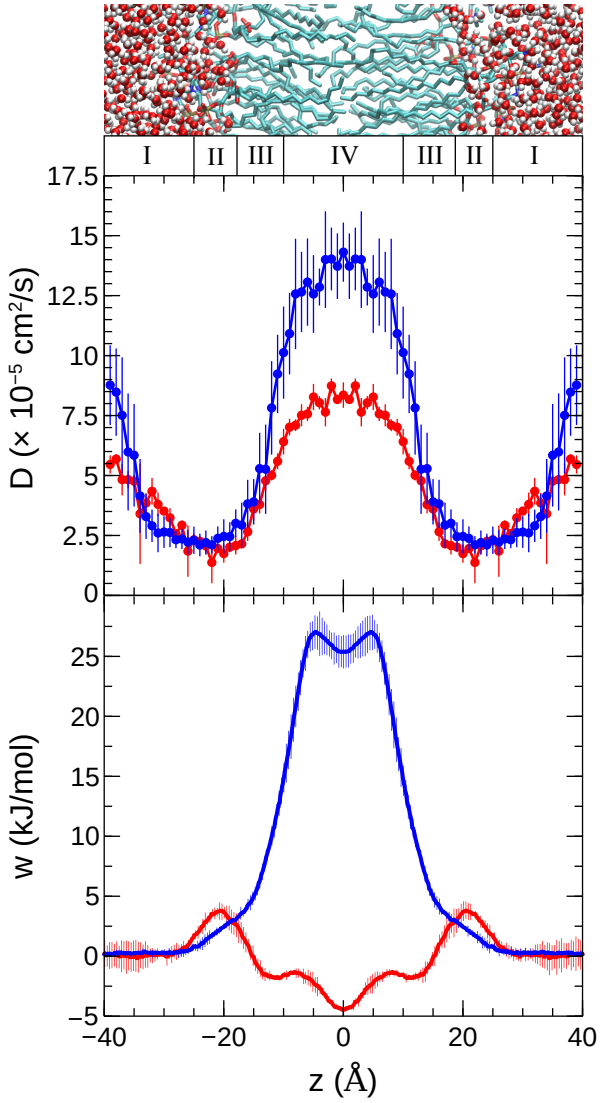

Figure 3: The diffusivity ($D(z)$, top) and potential of mean force ($w(z)$, bottom) of H_2O and O_2 permeating through a DPPC bilayer. The curves for H_2O are shown in blue while the curves for O_2 are shown in red. Simulations were performed at 323 K. The CHARMM36 lipid model and TIP3P water models were used. The PMF profiles were calculated from 20 ns H-REMD umbrella sampling simulations. The diffusivity profiles were calculated from the average of six 4 ns MD simulations using Eqn. 17.

solute moved across the bilayer. The enthalpy component disfavors partitioning of hexane at the center of the bilayer where it has weaker intermolecular interactions with the lower-density lipid tails, but this is counteracted by a more favorable entropy term because the solute has greater configurational freedom in the fluid-like bilayer center.

The PMF of water is typical for the permeation of a polar solute. The PMF of permeation for hydrophilic solutes do not show large changes in the headgroup or ester regions. These regions are easily accessible by the solvent, so the solutes are largely hydrated in these regions and can have stabilizing interactions with the head groups. The PMF increases abruptly when the solute enters the lipid chain region of the membrane (Region III). The PMF reaches a maximum in the lipid tail region (Region IV) that extends over 10 Å.

Permeation of charged and hydrogen-bonding solutes shows the most distinct PMFs, with a sharp peak at the center of the bilayer. These compounds remain partially hydrated by a finger of water molecules that extends from the headgroups into Regions III & IV. In permeation simulations of ionic compounds like Na^+, Cl^- (84), methylammonium (85), and methylguanidinium (86; 60; 87), the solute remains hydrated by a cluster of water molecules even at the center of the bilayer. Calculating the PMF is particularly challenging because various hydration states must be sampled. Because of this variable hydration, the motion of the solute cannot be reliably described as Brownian motion of a single particle, so the solubility-diffusion model is not necessarily a valid means to calculate a permeability coefficient. Nevertheless, the PMF can still be interpretively useful.

In one of the most extensive studies of nonfacilitated ion permeation, Vorobyov et al. used simulation and electrophysiological experiments to explore the permeation mechanisms of Na^+, K^+, Cl^-, and $GuanH^+$ (88). The PMFs were largely similar despite differences in size and charge, yielding similar membrane permeabilities that agree semiquantitatively with experiments in terms of magnitude and selectivity. The hydration of the ions inside the membrane negates the differences in the ion solvation energy that would be dominant in a traditional solubility-diffusion permeation mechanism. This led them to propose that permeation of ionic compounds occurs through a distinct, ion-induced permeation mechanism, where the ion induces a deformation in the membrane that allows the ion to permeate without being desolvated.

4.2. Connection to partition coefficients and the Meyer–Overton rule

A central tenet of the solubility-diffusion model is that the concentration at a given point, z, is determined by the equilibrium between the solute partitioning to the position z in the bilayer layer and the solution.

$$w(z) = -RT\ln K_{\mathrm{eq}}(z) \tag{21}$$

Due to the exponential dependence on $w(z)$ and the tendency for $w(z)$ to have a broad plateau at the center of the membrane, the permeability coefficient of a solute is largely determined by the value where $w(z)$ is a maximum. This suggests a proportionality between the log of the permeability coefficient and the equilibrium constant for the solute,

$$\log P_m \propto \ln K_{\mathrm{eq}}(z_{\mathrm{center}}). \tag{22}$$

As a solvation environment, the interior of the membrane is similar to a liquid alkane, so the equilibrium constant between the solvent and the center of the membrane will in turn be proportional to the alkane/water partition coefficient (P),

$$K_{\mathrm{eq}}(z_{\mathrm{center}}) \propto P_{\mathrm{alkane/water}} = \frac{[\mathrm{solute}]_{\mathrm{alkane}}}{[\mathrm{solute}]_{\mathrm{water}}} \tag{23}$$

Note the difference between the permeability coefficient, P_m, and the partition coefficient, P. P_m gives the rate of flux of a solute across the membrane through Eqn 1 and has units of distance per unit time. The partition coefficient is a measure of the relative concentration of the solute in two phases and is dimensionless.

The octanol/water and hexane/water partition coefficients are commonly used as measures for the degree to which a solute will partition into the membrane interior. It has been suggested that the octanol/water partition coefficient is a better measure for partitioning into the lipid headgroups than the membrane interior (89). Walter and Gutknecht showed that the hexadecane/water partition coefficient has the strongest correlation to membrane permeability, with a correlation coefficient of $r = 0.950$ (34). Based on this, the permeability coefficient and the alkane/water partition coefficients are closely related (i.e., $\log P_m \propto \log P_{\mathrm{hexadecane/water}}$), which provides a theoretical basis for the Meyer–Overton rule.

4.2.1. Diffusivity profiles

The diffusivity profiles of solutes follow some general trends. The diffusivity is high at the center of the membrane where the lipid tails are disordered and fluid-like. The diffusivity drops significantly in Region III, where the

lipid tails are ordered and undergo slow rearrangements (90). The diffusivity remains at a depressed value in the headgroup/water interface region, but increases again when the solute enters the solution (Region I). It should be noted that the diffusivity in the solution region will generally be overestimated by a factor of 2–3 when the TIP3P water model is used because this model has an erroneously low viscosity (91).

The diffusivity of larger permeants tends to be smaller than for smaller permeants. In Fig. 3, the diffusivity of the diatomic O_2 is systematically smaller than for H_2O, which has only one non-hydrogen atom. This can be interpreted using the Stokes–Einstein equation (71),

$$D = \frac{k_B T}{6\pi\eta r}, \tag{24}$$

which predicts that the diffusion coefficient of a solute in solution is inversely proportional to the molecular radius, r. The Stokes–Einstein diffusion coefficient also has an inverse dependence on the viscosity of the solvent (η), which predicts that solutes would diffuse more rapidly in low-friction regions of the bilayer.

Broadly speaking, the diffusivity of a solute varies by a factor of 5–6 across the bilayer. While this is a significant difference, the solubility-diffusion model permeability coefficient is only linearly dependent on the $D(z)$. As a result, the permeability of a solute is less sensitive to $D(z)$ than it is to $w(z)$, which has an exponential dependence. Furthermore, the high diffusivity in Region IV largely cancels the low diffusivity in Regions II & III. This generally supports the strategy of many researchers who have interpreted trends in permeability based only on the PMF; however, quantitative comparison to experimental permeability coefficients still require accurate calculations of

the diffusivity profiles.

4.3. Applications of the solubility-diffusion model

The 1994 paper by Marrink and Berendsen on the calculation of permeability coefficients from molecular simulation has been cited more than 500 times as of 2015 (43). The model has been used to describe the permeation of solutes ranging from gases to nanoparticles. Table A.2 in Appendix A summarizes 85 papers where membrane permeability is studied using molecular simulation.

Although many studies have focused on qualitative analysis of membrane permeability, there are many examples of quantitative calculations using the solubility-diffusion model. Orsi and Essex reported one successful example where the permeability of β-blocker drugs was calculated (92). A dual-resolution model was used to calculate permeability rankings of alprenolol, atenolol, pindolol, progesterone, and testosterone through DMPC lipid bilayers. In general, the permeability coefficients were predicted within an order of magnitude.

Another study by Riahi and Rowley employed the solubility-diffusion model to explain the high membrane permeability of hydrogen sulfide (H_2S). In this study, the authors employed all-atom polarizable molecular dynamics simulations to compute the permeability of H_2O and H_2S through a DPPC lipid bilayer. The calculated membrane permeability coefficients for both permeants were in good agreement with the experimental values.

Holland and coworkers studied the permeability of molecular oxygen and trace amine p-tyramine (charged and neutral) through model phosphatidylcholine (PC) lipid bilayers (93). The permeability of oxygen was studied at

two temperatures, 323 K and 350 K, while that of p-tyramine was studied at 310 K. The PMF and diffusion coefficient, $D(z)$, for the permeants were obtained using non-equilibrium work methods, which in turn were used to calculate the permeability coefficient of the permeants using the solubility-diffusion model. The calculated permeability coefficients for the selected permeants were in good agreement with experimental permeability of similar lipid bilayers.

4.4. Effect of cholesterol content

One of the most significant contributions of the solubility-diffusion model has been in understanding the effect of cholesterol on membrane permeability. Cholesterol is a major component of eukaryotic cell membranes and has a large effect on membrane permeability. Generally, solutes permeate membranes with higher cholesterol content at lower rates (94; 95; 96).

One of the earliest simulation studies on the effect of cholesterol content on membrane permeability was reported by Jedlovszky and Mezei (97). Simulations of 8 solutes (H_2O, O_2, CO, CO_2, NO, NH_3, $CHCl_3$, and formamide) permeating through DMPC bilayers with varying cholesterol concentration pointed to changes in the PMF as the cause of the reduced permeability. A later study by Hub et al. found that the PMF for the permeation of ammonia and carbon dioxide was increased when the cholesterol content of the membrane was high (98). The effect of cholesterol on the permeation of drug molecules has also been studied. Eriksson and Eriksson investigated the influence of cholesterol on the membrane permeability properties of the photodynamic drug, hypericin, and its mono- and tetra-brominated derivatives. The authors found that the calculated rate of permeation was lower

at high cholesterol content due to higher PMF barriers (99).

Several simulation studies have examined the effect of bilayer cholesterol content on water permeation, which also decreases at high cholesterol content (23). Saito and Shinoda explored the effect of cholesterol content on the water-permeation PMFs of DPPC and PSM lipid bilayers (100). They found that with increasing cholesterol concentration, both DPPC and PSM lipid membranes displayed an increased PMF for water permeability; although the effect was more prominent in the PSM bilayers with 30 mol % of cholesterol content. Similarly, Issack and Peslherbe examined the influence of cholesterol on the PMF and diffusivity profiles for transmembrane water permeation (101). They found that the PMF in Region III was significantly increased when the cholesterol content was high. A small decrease in diffusivity in Region IV had a secondary contribution.

Wennberg et al. reported a comprehensive study of the effect of cholesterol on permeation (48). The PMFs for solute permeation across 20 different lipid membranes containing one of four types of phospholipids (i.e., DMPC, DPPC, POPC, POPE) and cholesterol content that varied from 0 to 50 mol % were computed. The general trend from this study was that the PMFs for solute permeation were increased when the cholesterol content was high, particularly in Region III, where the ring structure of cholesterol preferentially partitioned. Cholesterol is relatively rigid and packs tightly into the lipid tails, resulting in strong London dispersion interactions between the lipids and the cholesterol. A permeating solute disrupts these interactions and is generally unable to pack into the lipid tails as tightly as can cholesterol. As a result, the PMF for a solute permeating through Region III of a cholesterol-

containing bilayer is increased, which decreases the rate of permeation. A subsequent study by Zocher et al. found the diffusivity of permeating solutes were generally independent of cholesterol content and changes in the PMF were the dominant effect on permeation rates (102).

4.4.1. Lipid composition

The effect of lipid composition of permeation has also been studied computationally. These studies have primarily used model amino acid side chains as the solutes because the partitioning of side chains into the interior of a membrane is relevant to membrane protein structure and function.

One notable study by Li et al. investigated the role of membrane thickness in saturated phosphatidylcholine (PC) lipid bilayers (85). The authors calculated the PMFs for the permeation of arginine side chain analog $MguanH^+$ across PC lipid bilayers with increasing thickness (DSPC, DPPC, DMPC, DLPC, DDPC). The authors proposed that an ion-induced defect mechanism is the principal means of arginine translocation within lipid bilayers with lipid tails up to 18 carbons in length (e.g., DSPC). For thicker bilayers, the solubility-diffusion mechanism is preferred.

The results for protonated methylguanidinum ($MguanH^+$), a model for an arginine side chain, were particularly significant. For all lipid bilayers used in the study, similar membrane deformations were observed for $MguanH^+$ translocation; where water and lipid head groups are drawn into the hydrophobic core of the bilayer. The free energy barrier for $MguanH^+$ translocation in lipid bilayers display a systematic dependence on membrane thickness with predictable shifts between bilayers of increasing thickness. Narrow transmembrane pores and corresponding plateaus in free energy profiles are

observed for MguanH$^+$ translocation across thin membranes (DDPC, DLPC) suggesting a favorable energetic cost for burying an arginine residue into a thin bilayer; a finding that is consistent with experimental measurements (103). This work indicates that membrane thickness plays an important role in the membrane partitioning of charged amino acid side chains.

The effect of lipid headgroup and tail length of side chain partitioning was also studied by Johannson and Lindahl using molecular simulation (104). The PMFs for permeation of 8 side chain models (Asp, Glu, Arg, Lys, Ser, Trp, Leu, and Phe) was calculated for six different types of bilayer (DMPC, DOPC, DOTAP, POPC, POPE, and POPG) with different head and tail groups. The PMF barriers of polar and charged groups were higher and broader for thicker membranes, but PMF barriers for hydrophobic groups were lower. The charge of the lipid head group had a large effect on the permeation of charged compounds. The barriers for Glu and Arg side chains increased as the lipids were changed from cationic, to zwitterionic, to anionic headgroups.

5. Innovations in modeling permeation

5.1. Polarizable models

Permeating solutes pass from the polar aqueous phase through the nonpolar membrane interior. In the course of permeation, the dielectric constant changes from $\epsilon = 78$ in bulk water to $\epsilon = 2$ in the lipid tail region. Polarizable solutes can experience a large induced polarization when dissolved in liquid water. This polarization effectively disappears when the solute moves to the nonpolar membrane interior. For solutes that can hydrogen-bond with

water, this change in polarization is even more significant because the solutes experience a large electric field from the water molecules. Most simulations to date use fixed atomic charges to describe electrostatic interactions, so they are incapable of describing the effects of induced polarization.

Force fields that include the effects of induced polarization are gradually becoming available. A variety of polarizable models for biomolecules have been developed, including the Drude (105; 106), CHarge EQuilibration Method (CHEQ) (107), and the Atomic Multipole Optimized Energetics for Biomolecular Simulation (AMOEBA) models (108). Drude models are attractive for bilayer simulations because of their efficiency; polarizability is incorporated by tethering charged "Drude" particles to non-hydrogen atoms and propagating their positions dynamically (see Fig. 4), so there is no additional iterative process to calculate the charge distribution.

To date, only a handful of polarizable force fields for lipids are available. Davis et al. reported a CHEQ polarizable model for DPPC lipids (109). Separately, Robinson has developed a Drude model force field for cholesterol and sphingomyelin (110). Harder et al. developed a Drude polarizable model for DPPC to model the lipid monolayer-air interface (111). Chowdhary et al. refined this model to describe DPPC bilayers (112). It should be noted that this Drude DPPC model is actually less accurate in describing the lipid head group area and order parameters than the nonpolarizable CHARMM36 model (112), although this can likely be addressed by further refinement of the force field parameters.

A simulation of water permeation through a DMPC bilayer using a CHEQ model was reported by Bauer et al., who found the barrier in the PMF using

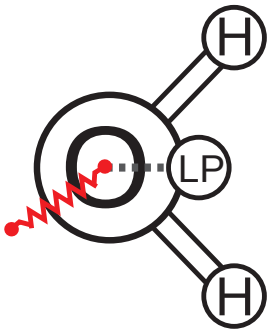

Figure 4: A schematic of the SWM4-NDP Drude polarize water molecule. Each water is comprised of three atomic centers (an oxygen and two hydrogens), a massless "lone-pair" particle is constrained to a position along the H–O–H bisector, and a negatively charged "Drude" particle that is tethered to the oxygen atom with a harmonic potential (red).

various CHEQ polarizable models to be in the 19–23 kJ/mol range (113). This barrier is somewhat lower than the 26–30 kJ/mol barriers reported in other simulations (113). The permeability coefficient was not calculated in this study, so this result cannot be directly tested by comparison to the experimental value. There was a large change in polarization of the permeating water molecule; the dipole moment of water dropped from 2.6 D in bulk water to 1.88 D at the bilayer center.

Riahi and Rowley simulated the permeation of H_2O and H_2S through a DPPC bilayer using the Drude polarizable model (49). The average dipole moment of H_2O decreased from 2.5 D to 1.9 D when it crossed into the center of the membrane interior, but the average dipole moment of H_2S only decreased from 1.2 D to 1.0 D. This is contrary to the trend in solute polarizability, as H_2S has a polarizability of 3.6 $Å^3$, while water has a polarizability of 1.45 $Å^3$ (Fig. 5). Counter-intuitively, molecules that are highly polarizable

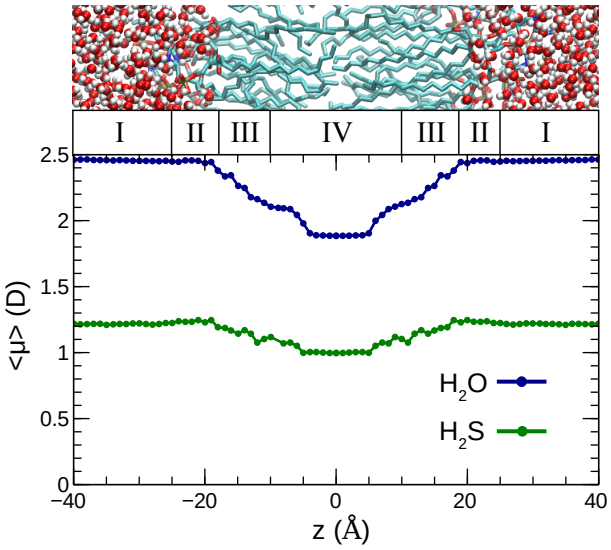

Figure 5: The dipole moments of H_2O (blue) and H_2S (green) solutes permeating across a DPPC bilayer. The average dipole of H_2O is high in solution ($\langle\mu\rangle = 2.5$ D) but drops to a value equal to its gas-phase dipole moment ($\mu_0 = 1.8$ D) at the center of the bilayer. H_2S experiences a much smaller change ($\langle\mu\rangle = 1.2 \rightarrow 1.0$ D) The values are averaged from the umbrella sampling windows, calculated with a Drude polarizable model. Data from Ref. 49.

will not necessarily be strongly polarized in liquid water because high polarizability correlates to larger molecular radii. In the case of H_2S, the modest polarity and large radius of the sulfur atom precludes hydrogen bonding or other kinds of close-range polarizing interactions with water. Induced polarization is most significant in molecules that have a large static dipole moment and form hydrogen bonds with water molecules.

Although the rigorous inclusion of induced polarization is desirable conceptually, the results from simulations using polarizable models are not necessarily more accurate. For instance, the water-permeation PMF calculated using the Drude model is very similar to that calculated using many nonpolarizable models. Nonpolarizable force fields are often parameterized to reproduce the experimental solvation free energies of solutes. These energies correspond to the change in Gibbs energy when the solute is transferred from the gas phase to liquid water, which involves a similar change in solute polarization to what occurs during membrane permeation. These nonpolarizable models will have the effect of induced polarization "baked in" through the parameterization, so the PMF barrier will be similar despite the neglect of induced polarization. For example, the permanent dipole moments of molecules described with the nonpolarizable GAFF model are systematically larger than the experimental gas phase values because of a systematic bias in the quantum chemical method used to assign the atomic charges (54; 114). In effect, this method of parameterization mimics the effect of induced polarization, although the physical basis for this is not entirely realistic. Likewise, the accuracy of a polarizable model is only as good as its parameterization.

Polarizable force fields can provide some other advantages for modeling

permeation. Because of the larger parameter space and more physically realistic description of the system, they can be parameterized to describe a greater range of properties with greater accuracy. For instance, the SWM4-NDP Drude polarizable water model provides good descriptions of the dielectric constant and diffusion coefficients of water (115). Some popular nonpolarizable water models, like TIP3P, are significantly in error for the calculation of these properties. The water permeation rate calculated by Riahi and Rowley using the Drude model was in quantitative agreement with experiment, suggesting that the solubility-diffusion model combined with a Drude polarizable force field is an effective method for modeling permeation (49). Developing lipid models for use with more accurate nonpolarizable water models, like TIP4P/2005 (116; 117), would address some of these limitations without requiring the use of polarizable models. Future development of both polarizable and nonpolarizable models for membrane permeation would benefit from being validated against the solvation energies and diffusion coefficients of the solutes in water and the liquid alkanes used to parameterize the lipid tails.

There are also several drawbacks associated with the use of polarizable force fields. The number of molecules that have been parameterized for simulations using polarizable force fields still lags behind established nonpolarizable force fields. The computational cost of polarizable models is greater than nonpolarizable force fields due to the need to calculate additional force field terms. Depending on the size and composition of the system, this can range from a factor of 4 for the Drude model to a factor of 20 for the AMOEBA model. Standard dual-Lagrangian implementations of the Drude model are

also incompatible with replica exchange methods. As a result, the benefits of using a polarizable model must be weighed against increased statistical error because the configurational sampling is more limited.

Simulations of membrane permeation using polarizable models are now possible for select solutes and lipids. The development of polarizable models for additional solutes and lipids will extend this further in the coming years. These models will make it possible to quantitatively examine the role of polarization in membrane permeation and could allow a greater level of accuracy in cases where induced polarization is significant. The choice between a nonpolarizable or a polarizable model depends on the availability and accuracy of the force fields and whether sufficient sampling can be performed using the polarizable model.

5.2. Coarse grain models

Coarse grain models have also been used to simulate membrane permeation. These models reduce the computational expense of the simulation by using a simplified description of intermolecular interactions and grouping atoms into "bead" particles. The MARTINI model for lipids has been notably successful in describing many of the physical properties of bilayers (118; 119). Groups of atoms of a bilayer system are transformed into bead particles. Each bead represents 3–4 non-hydrogen atoms of the lipid or solvent (Fig. 6). The nonbonded interaction potentials of the various types of bead particles are parameterized to reproduce the partitioning of solutes between various solvents (e.g., water–octanol). From this basic design, the surfactant properties of the bilayer arise intrinsically.

Through coarse graining, much of the atomic-scale resolution of the sys-

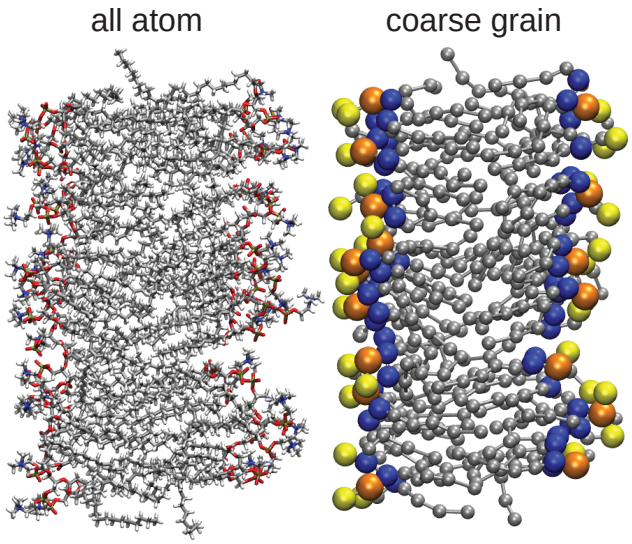

Figure 6: An all-atom POPC model bilayer (left) vs a MARTINI coarse grain model (right). Groups of 3–4 non-hydrogen atoms and the hydrogens bound to them are combined into a single "bead" particle in the coarse grain model.

tem is lost. Despite this, the description of many bilayer physical and dynamic properties relevant to permeation is remarkably good. For example, the viscosity coefficient of MARTINI water is 7×10^{-4} Pa·s (at 323 K), in fairly good agreement with the experimental value of 5.5×10^{-4} Pa·s (120). The self-diffusion coefficients predicted by this model are more variable; the rate of diffusion of water and alkanes are in good agreement with experiment, but alcohols and lipids diffuse at rates up to 20 times faster than experiment (121). The water permeability of a MARTINI DPPC bilayer was estimated by direct simulation to be 1.5×10^{-3} cm/s, which is a reasonable value given the simplicity of the model (118).

Coarse grain models have been used to study many of the same solutes that have been studied using all atom models, including H_2O, gases, ions,

and small organic molecules. Coarse grain models are particularly suitable for modeling permeation of nano-scale solutes that would be difficult to simulate at an appropriate scale with an atomistic model. These studies have included the permeation and partitioning of fullerenes and nanoparticles. These studies are summarized in Table 1.

For molecules that are too small to be coarse grained without losing significant aspects of their chemical properties, multiscale models may be effective. Orsi and Essex developed a model where the permeant was described by an all-atom model but the solution and bilayer were coarse grain (92). This model was generally effective at reproducing the permeability coefficients predicted by all-atom models.

Coarse grain models can be more computationally efficient than all atoms models by multiple orders of magnitude. Consequently, coarse grain simulations of permeation commonly include hundreds of lipids and simulations that are hundreds of nanoseconds long are routine. This is particularly significant when modeling large solutes that require large simulation cells and extensive sampling to calculate accurate $w(z)$ and $D(z)$ profiles. This advantage must be weighed against the loss of atomic detail in the model and quality of the coarse grain model used.

6. Conclusions

Molecular simulation has contributed significantly to the study of nonfacilitated membrane permeability. These simulations provide atomistic-scale insight into why solutes cross membranes at different rates and why the composition of the membrane affects permeability. The solubility-diffusion

Table 1: Papers using coarse grain models to simulate membrane permeation.

Year	Ref.	Subject	Lipid
2007	122	effect of bilayer stretching on water permeation	DPPC
2008	123	permeation of fullerene	DPPC
2009	124	permeability of Xe, O_2, and CO_2	DCPC, DMPC, and DPPC
2009	74	permeability of acetamide, acetic acid, benzene, ethane, methanol, methylacetate, methylamine water	DMPC
2009	125	permeation of fullerene and fullerene derivatives	DPPC
2010	126	permeation of Na^+ and K^+	DPPC
2010	127	permeation of water	DPPC and MPPC
2010	92	pharmaceuticals (alprenolol, atenolol, and pindolol) and hormones (progesterone and testosterone)	DMPC
2012	128	Permeation of nanoparticle and nanoparticle with hydrophobic coating	DPPC
2012	129	Effect of nanoparticle size and velocity on membrane during permeation	DPPC
2013	130	nanoparticle with hydrophobic and hydrophilic coating	DPPC
2015	131	effect of surface functionalization of nanoparticles on permeation	DPPC

model has provided a method for the quantitative calculation of permeability coefficients from the potential of mean force and diffusivity profiles of the solutes on the transmembrane axis. Although accurate calculation of these profiles can be challenging, there are established computational strategies for computing them. More sophisticated molecular mechanical force fields will improve the accuracy of the underlying models. More representative configurational sampling through improvements in computing hardware and more efficient simulation algorithms will reduce statistical error. Coarse grain and polarizable force fields have promise in addressing the sampling issues and accuracy of permeation simulations, respectively. Experimental permeability measurements often rely on complex models and can involve complex bilayer compositions, so direct comparisons to experimental data are not always straightforward. Once these issues are resolved, the quantitative accuracy of the underlying solubility-diffusion model can also be assessed.

There are many interesting subjects in nonfacilitated membrane permeation that remain unexplored. The success of molecular simulation in describing the effect of cholesterol content on permeability suggests that these techniques could be used to understand the effects of other aspects of membrane composition on permeability. Notably, most studies to date have used pure DPPC bilayers as a membrane model and simulations using mixed-lipid bilayers that are more representative of biological cell membranes have not been reported yet. Simulations may also be able to help resolve the controversy over purported exceptions to the Meyer–Overton rule (25; 132; 133; 134; 26).

Cell membranes are remarkable structures that emerge from the amphiphilic properties of the constituent lipids. The selective permeability of

lipid bilayers is ultimately a simple phase partitioning effect that arises from complex intermolecular interactions. Appropriately, the solubility-diffusion model is a simple but effective theory for understanding the complex process of permeability. Marrink and Berendsen's 1994 paper that first demonstrated that permeability coefficients could be calculated quantitatively using molecular dynamics simulations has been cited over 500 times in the last 21 years and is undoubtedly a landmark paper in computational biophysics (43).

Acknowledgements

We thank NSERC of Canada for funding through the Discovery Grant program (Application 418505-2012). EAW thanks ACEnet and Memorial University for funding. Computational resources were provided by Compute Canada (RAPI: djk-615-ab) through the Calcul Quebec and ACEnet consortia. We thank Dr. Chris Neale and the reviewers for helpful comments.

Appendix A. Summary of membrane permeability simulations

Table A.2: Papers using molecular simulation to model nonfacilitated membrane permeation

Year	Ref.	Subject	Lipid
1994	43	permeation of H_2O	DPPC
1996	83	permeation of O_2, NH_3, and Lennard-Jones spheres	DPPC
1996	135	permeation of Na^+ and Cl^-	GMO

1998	136	effects of halothane on lipid bilayer structure	DPPC
2000	137	permeability of H_2O, O_2, CO, CO_2, NO, $CHCl_3$	DMPC
2001	138	permeation of ubiquinone	DPPC
2002	139	permeability of organic molecules (antipyrine, caffeine, ganciclovir, α-D-glucose)	dodecane chains
2003	140	permeation of valproic acid	DPPC
2003	97	effect of cholesterol on the permeability of small molecules (H_2O, O_2, CO, CO_2, NO, NH_3, $CHCl_3$, and CH_3NO)	DMPC
2003	141	permeation of oxygen	DMPC
2004	142	interactions of water molecules with lipid membranes	PCs/PEs
2004	90	permeation of small organic molecules (acetamide, acetic acid, benzene, ethane, methanol, methyl acetate, methylamine, water)	DPPC
2004	143	effects of chain branching on water and neutral solute permeability	DPPC/DPhPC
2004	144	permeation and effects of pentachlorophenol (PCP)	POPE/POPC
2004	145	effects of ether- and ester-linked lipid bilayers on solute (H_2O and O_2) permeability	ether-DPhPC/ester-DPhPC
2005	146	permeation and interaction of pyrene	POPC

2005	147	permeation of small solutes (acetic acid, benzene, ethane, methanol, methyl acetate, methylamine, water) and large drugs (alprenolol, atenolol, pindolol)	DPPC
2005	148	effects of lipid hydrocarbon chain length on oxygen, water and nitric oxide permeability	DLPC/DMPC/DPPC
2005	149	influence of different drug transport routes	Caco-2, 2/4/A1, hexadecane membrane models
2006	150	permeation of hexane	DOPC
2006	151	localization and orientation of indole and benzene	POPC
2007	152	permeation of water	POPC/ DOPC/ DMPC/ DLPC/ diC22:1PC/ DOPS/ DLPE
2008	123	permeation of fullerene and effects on membrane properties	DOPC/ DPPC
2008	153	permeation of amino acids	DOPC

2008	154	permeability of water	POPC / DOPC / DMPC / DLPC / diC22:1PC
2008	155	permeation of water	8-carbon alkyl-phenol poly-oxyethy-lene/ oleate
2008	156	permeability and behavioral effects of 5-aminolevulunic acid and its ester derivatives	DPPC
2008	157	permeation of water	DPhPC
2008	158	permeation of O_2 and CO_2	POPE
2008	159	effects of halothane as a function of pressure in different membrane depths	DMPC
2009	84	permeation of Na^+ and Cl^-	DMPC
2009	160	permeability of water	DMPC
2009	161	permeation of ribose, aribinose and xylose	POPC
2009	162	permeation of water	CER2 bi-layer
2009	163	permeation of sulfur mustard and heptane	DPPC
2009	164	permeation of NO	PC/PE

2009	165	effects of carbon nanoparticles on lipid membranes	DPPC/DMPC
2010	166	permeation of drugs (alprenolol, atenolol, pindolol) and hormones (progesterone, testosterone)	DMPC
2010	167	permeation of aspirin and ibuprofen	DPPC
2010	168	permeation of buckyball-sized nanoparticles	DMPC
2010	98	permeation of NH_3 and CO_2	POPE/ 3:1 POPE:POPG/ 1:1 POPE:POPC/ POPC
2011	169	predictive modeling of skin permeation	ceramide class of lipids
2011	170	permeation of nanoparticles with mixed hydrophobic/ hydrophilic surface functionalization	hydrophilic/ hydrophobic beads
2011	100	effect of cholesterol on water permeability	DPPC/ PSM
2011	99	influence of cholesterol on the permeability of hypericin and its brominated derivatives	DPPC
2011	166	permeation of triclocarbon and triclosan	DOPC
2011	113	permeation of water	DMPC
2011	171	permeation of nucleosides	POPC

2011	172	permeation of benzo[b]-thiophene-2-boronic acid (BZB)	POPC
2012	48	effect of cholesterol on partitioning of ethanol, ammonia, nitric oxide, propane, benzene, and pentane	POPE/ POPC/ DMPC/ DPPC
2012	173	partitioning of couramin	DOPC
2012	174	permeation of tryptophan	DOPC
2012	175	permeation of ethanol molecules	POPC
2012	176	permeation and structural influence of ibubrofen	DOPC
2012	177	effect of DMSO on water permeability	DMPC
2012	178	permeation of methane and water molecules	SDS micelles
2012	179	effect of anesthetic molecules on lipid membrane properties	DPPC
2012	180	permeation of water	DPPC
2013	181	permeation and chemical approaches of molecules in breaching skin lipid barrier	ceramide skin lipid
2013	47	permeation of n-propylguanidinium	POPC

2013	182	permeability of cytochrome P450 substrates (caffeine, chlorzaxazone, couramin, ibuprofen, debrisoquine) and metabolites (paraxanthine, 6-hydroxychlorzoxazone, 7-hydroxycoumarin, 3-hydroxyibuprofen, 4-hydroxydebrisoquine)	DOPC/ POPG
2013	183	permeation of fullerene-like nanoparticles	DPPC
2013	184	permeation of nanoparticles with hydrophobic-hydrophilic surface patterns	DPPC
2013	185	permeability prediction of candidate drug compounds	DMPC
2013	186	permeation of N-acetyl-L-tryptophanamide (NATA)	DOPC
2013	187	permeation of argenteane and 3,3'-dimethoxy-1,1'-biphenyl-2,2'-diol	DOPC/PLPC
2013	188	permeability analysis of selected molecules	egg lecithin/DMPC
2013	189	permeation of water	DOPC/ DPPC/ DOPS/ 9:1 DOPC:DPPC/ 3:1 POPG:POPE
2013	190	permeation and structural diversity of warfarin	DOPC

2013	191	permeation of water	DPPC/ DLPS
2013	102	effect of cholesterol on solute (NH_3, pyridine, TEA, NO) permeability	DOPE/ DOPC/ PLE
2013	192	permeation of polystyrene nanoparticles	DPPC
2014	49	permeation of H_2S and H_2O	DPPC
2014	193	interaction and permeation properties of paclitaxel	POPC
2014	194	permeation of methyldopa	POPC
2014	195	interactions and permeation properties of neurotransmitters (GABA, GLY, ACH, GLU)	DPPC
2014	69	permeation of water/ethanol	POPC
2014	196	permeability of reactive oxygen species (O_2, singlet oxygen, O_2^-, H_2O_2, HO, HO_2)	POPC
2014	197	influence of cholesterol on ibuprofen permeation	DMPC
2015	93	permeation of O_2 and p-tyramine	DPPC/ PC bilayers
2015	198	permeation of tryptophan molecule	DOPC
2015	199	permeation and effect of circumin in lipid bilayers	DMPG/ DPPC
2015	101	effect of cholesterol on water permeability	DPPC

2015	200	effect of lipid phase composition on particle permeation	model system (a group of neutral five-site molecules)
2015	201	effect of ethanol on water transport properties of CER2 bilayers	CER2
2015	202	permeation of dioxin	DPPC

DPPC: 1,2-dipalmitoyl-sn-glycero-3-phosphocholine, POPC: 1-palmitoyl-2-oleoyl-sn-glycero-3-phosphocholine, DMPC: 1,2-dimyristoyl-d54-sn-glycero-3-phosphocholine, CER2: N-lignoceroyl-D-erythro-sphingosine, DOPC: 1,2-dioleoyl-sn-glycero-3-phosphocholine, POPE: 1-palmitoyl-2-oleoyl-sn-glycero-3-phosphoethanolamine, DLPC: 1,2-didodecanoyl-sn-glycero-3-phosphocholine, DMPG: 1,2-dimyristoyl-sn-glycero-3-phospho-(1'-rac-glycerol), DLPS: 1,2-dilauroyl-sn-glycero-3-phospho-L-serine, POPG: 1-palmitoyl-2-oleoyl-sn-glycero-3-phospho-(1'-rac-glycerol)

Appendix A. Technical details

The simulations of H_2O and O_2 permeation were performed using NAMD 2.10 (203). The CHARMM36 lipid force field was used to represent the DPPC lipids (53). The TIP3P model was used to represent the water molecules (50). The Fischer–Santiago model was used for O_2. The bilayer model was comprised of 4551 water molecules and 64 DPPC lipids. All bonds containing a hydrogen atom were constrained using the SHAKE algorithm (204). A 2 fs time step was used.

The trajectory of O_2 permeation was calculated from an equilibriated system where the O_2 molecule was in solution. An 10 ns NVE simulation was initiated. The 300 ps section where the O_2 molecule permeates the membrane is presented in Fig. 1.

The PMFs ($w(z)$) presented in Fig. 3 were calculated from 20 ns replica exchange umbrella sampling simulation. Each replica corresponded to a NPT simulation of the system where the position of the solute along the z-axis was restrained using a harmonic potential (Eqn. 11). The replicas were at 1 Å intervals along the z axis over the range $z = [-40$ Å, 40 Å$]$ for a total of 81 replicas. A force constant of $k = 5$ kcal Å^2 was used for all windows. Exchanges between neighboring replicas were attempted every 1000 time steps. $w(z)$ was calculated from the probability distributions of these profiles using the weighted histogram analysis method (WHAM) (205; 62). The diffusivity profiles were calculated from the average of six 4 ns MD simulations using Eqn. 17.

References

[1] M. Edidin, Lipids on the frontier: a century of cell-membrane bilayers, Nat. Rev. Mol. Cell Biol. 4 (5) (2003) 414–418. doi:10.1038/nrm1102.

[2] G. van Meer, D. R. Voelker, G. W. Feigenson, Membrane lipids: where they are and how they behave, Nat. Rev. Mol. Cell Biol. 9 (2) (2008) 112–124. doi:10.1038/nrm2330.

[3] N. Ridgway, R. McLeod, Functional roles of lipids in membranes, in: Biochemistry of Lipids, Lipoproteins and Membranes, Elsevier Science, 2015, pp. 1–39.

[4] B. Hille, Ion Channels of Excitable Membranes (3rd Edition), 3rd Edition, Sinauer Associates Inc 2001-07, 2001.

[5] M. Luckey, Membrane Structural Biology: With Biochemical and Biophysical Foundations, Cambridge University Press, 2008.

[6] B. Roux, S. Bernèche, B. Egwolf, B. Lev, S. Y. Noskov, C. N. Rowley, H. Yu, Ion selectivity in channels and transporters, J. Gen. Physiol. 137 (5) (2011) 415–426. doi:10.1085/jgp.201010577.

[7] A. Volkov, S. Paula, D. Deamer, Two mechanisms of permeation of small neutral molecules and hydrated ions across phospholipid bilayers, Bioelectrochemistry and Bioenergetics 42 (2) (1997) 153–160, 13th International Symposium on Bioelectrochemistry and Bioenergetics. doi:10.1016/S0302-4598(96)05097-0.

[8] G. Camenisch, J. Alsenz, H. van de Waterbeemd, G. Folkers, Estimation of permeability by passive diffusion through caco-2 cell monolayers using the drugs' lipophilicity and molecular weight, Eur. J. Pharm. Sci. 6 (4) (1998) 313–319. doi:10.1016/S0928-0987(97)10019-7.

[9] M. Kansy, F. Senner, K. Gubernator, Physicochemical high throughput screening: Parallel artificial membrane permeation assay in the description of passive absorption processes, J. Med. Chem. 41 (7) (1998) 1007–1010. doi:10.1021/jm970530e.

[10] H. Liu, C. Sabus, G. Carter, C. Du, A. Avdeef, M. Tischler, In vitro permeability of poorly aqueous soluble compounds using different solubilizers in the pampa assay with liquid chromatography/mass spectrometry detection, Pharmaceutical Research 20 (11) (2003) 1820–1826.

[11] S. Paula, A. G. Volkov, A. N. V. Hoek, T. H. Haines, D. W. Deamer, Permeation of protons, potassium ions, and small polar molecules through phospholipid bilayers as a function of membrane thickness, Biophys. J. 70 (1) (1996) 339–348. doi:10.1016/S0006-3495(96)79575-9.

[12] Y. Antonenko, P. Pohl, G. Denisov, Permeation of ammonia across bilayer lipid membranes studied by ammonium ion selective microelectrodes, Biophys. J. 72 (5) (1997) 2187–2195. doi:10.1016/S0006-3495(97)78862-3.

[13] Y. Antonenko, G. Denisov, P. Pohl, Weak acid transport across bilayer

lipid membrane in the presence of buffers. theoretical and experimental ph profiles in the unstirred layers, Biophys. J. 64 (6) (1993) 1701–1710. doi:10.1016/S0006-3495(93)81542-X.

[14] J. C. Mathai, A. Missner, P. K"ugler, S. M. Saparov, M. L. Zeidel, J. K. Lee, P. Pohl, No facilitator required for membrane transport of hydrogen sulfide, Proc. Natl. Acad. Sci. U.S.A. 106 (39) (2009) 16633–16638. doi:10.1073/pnas.0902952106.

[15] F. Antunes, E. Cadenas, Estimation of H_2O_2 gradients across biomembranes, FEBS Lett. 475 (2) (2000) 121–126. doi:10.1016/S0014-5793(00)01638-0.

[16] G. P. Bienert, J. K. Schjoerring, T. P. Jahn, Membrane transport of hydrogen peroxide, Biochimica et Biophysica Acta (BBA) - Biomembranes 1758 (8) (2006) 994–1003. doi:10.1016/j.bbamem.2006.02.015.

[17] W. K. Subczynski, M. Lomnicka, J. S. Hyde, Permeability of nitric oxide through lipid bilayer membranes, Free Radical Res. 24 (5) (1996) 343–349. doi:10.3109/10715769609088032.

[18] S. Nedeianu, T. Pli, D. Marsh, Membrane penetration of nitric oxide and its donor s-nitroso-n-acetylpenicillamine: a spin-label electron paramagnetic resonance spectroscopic study, Biochim. Biophys. Acta - Biomembranes 1661 (2) (2004) 135–143. doi:10.1016/j.bbamem.2003.12.008.

[19] J. Widomska, M. Raguz, W. K. Subczynski, Oxygen permeability of the lipid bilayer membrane made of calf lens lipids, Biochimica et

Biophysica Acta (BBA) - Biomembranes 1768 (10) (2007) 2635–2645. doi:10.1016/j.bbamem.2007.06.018.

[20] W. K. Subczynski, J. S. Hyde, A. Kusumi, Oxygen permeability of phosphatidylcholine–cholesterol membranes, Proc. Natl. Acad. Sci. U.S.A. 86 (12) (1989) 4474–4478.

[21] M. S. Al-Abdul-Wahid, C.-H. Yu, I. Batruch, F. Evanics, R. Pomès, R. S. Prosser, A combined nmr and molecular dynamics study of the transmembrane solubility and diffusion rate profile of dioxygen in lipid bilayers, Biochemistry 45 (35) (2006) 10719–10728. doi:10.1021/bi060270f.

[22] E. Terreno, A. Sanino, C. Carrera, D. D. Castelli, G. B. Giovenzana, A. Lombardi, R. Mazzon, L. Milone, M. Visigalli, S. Aime, Determination of water permeability of paramagnetic liposomes of interest in {MRI} field, J. Inorg. Biochem 102 (5–6) (2008) 1112 – 1119. doi:10.1016/j.jinorgbio.2008.01.025.

[23] J. C. Mathai, S. Tristram-Nagle, J. F. Nagle, M. L. Zeidel, Structural determinants of water permeability through the lipid membrane, J. Gen. Phys. 131 (1) (2008) 69–76. doi:10.1085/jgp.200709848.

[24] A. Sigler, P. Schubert, W. Hillen, M. Niederweis, Permeation of tetracyclines through membranes of liposomes and escherichiacoli, Euro. J. Biochem. 267 (2) (2000) 527–534. doi:10.1046/j.1432-1327.2000.01026.x.

[25] A. V. Thomae, H. Wunderli-Allenspach, S. D. Krmer, Permeation of aromatic carboxylic acids across lipid bilayers: The ph-partition hypothesis revisited, Biophys. J. 89 (3) (2005) 1802–1811. doi:10.1529/biophysj.105.060871.

[26] A. Missner, P. Pohl, 110 years of the meyer–overton rule: Predicting membrane permeability of gases and other small compounds, ChemPhysChem 10 (9-10) (2009) 1405–1414. doi:10.1002/cphc.200900270.

[27] J. Gutknecht, D. C. Tosteson, Diffusion of weak acids across lipid bilayer membranes: Effects of chemical reactions in the unstirred layers, Science 182 (4118) (1973) 1258–1261. doi:10.1126/science.182.4118.1258.

[28] P. Pohl, S. M. Saparov, Y. N. Antonenko, The size of the unstirred layer as a function of the solute diffusion coefficient, Biophys. J. 75 (3) (1998) 1403–1409.

[29] S. Mitragotri, M. E. Johnson, D. Blankschtein, R. Langer, An analysis of the size selectivity of solute partitioning, diffusion, and permeation across lipid bilayers, Biophys. J. 77 (3) (1999) 1268–1283. doi:10.1016/S0006-3495(99)76978-X.

[30] A. Mälkiä, L. Murtomäki, A. Urtti, K. Kontturi, Drug permeation in biomembranes: In vitro and in silico prediction and influence of physicochemical properties, Eur. J. Pharm. Sci. 23 (1) (2004) 13–47. doi:10.1016/j.ejps.2004.05.009.

[31] B. Faller, Artificial membrane assays to assess permeability, Curr. Drug Metab. 9 (2008) 886–892.

[32] H. Meyer, Zur theorie der alkoholnarkose, Archiv für experimentelle Pathologie und Pharmakologie 42 (2–4) (1899) 109–118. doi:10.1007/BF01834479.

[33] C. E. Overton, Studien über die Narkose; zugleich ein Beitrag zur allgemeinen Pharmakologie, Jena, Fischer, 1901.

[34] A. Walter, J. Gutknecht, Permeability of small nonelectrolytes through lipid bilayer membranes, J. Membr. Biol. 90 (3) (1986) 207–217. doi:10.1007/BF01870127.

[35] I. Bloch, A theory of membrane permeability: I, The bulletin of mathematical biophysics 6 (3) (1944) 85–92. doi:10.1007/BF02478238.

[36] H. Träuble, The movement of molecules across lipid membranes: A molecular theory, J. Memb. Biol. 4 (1) (1971) 193–208. doi:10.1007/BF02431971.

[37] A. Finkelstein, Water and nonelectrolyte permeability of lipid bilayer membranes, J. Gen. Physiol. 68 (1976) 127–135.

[38] J. L. MacCallum, D. P. Tieleman, Chapter 8 interactions between small molecules and lipid bilayers, in: S. E. Feller (Ed.), Computational Modeling of Membrane Bilayers, Vol. 60 of Current Topics in Membranes, Academic Press, 2008, pp. 227–256. doi:10.1016/S1063-5823(08)00008-2.

[39] M. Orsi, J. W. Essex, Chapter 4 passive permeation across lipid bilayers: a literature review, in: Molecular Simulations and Biomembranes: From Biophysics to Function, The Royal Society of Chemistry, 2010, pp. 76–90. doi:10.1039/9781849732154-00076.

[40] D. G. Levitt, Interpretation of biological ion channel flux data–reaction-rate versus continuum theory, Annu. Rev. Biophys. Biophys. Chem. 15 (1) (1986) 29–57. doi:10.1146/annurev.bb.15.060186.000333.

[41] T. W. Allen, O. S. Andersen, B. Roux, Energetics of ion conduction through the gramicidin channel, Proc. Natl. Acad. Sci. U.S.A. 101 (1) (2004) 117–122. doi:10.1073/pnas.2635314100.

[42] J. M. Diamond, Y. Katz, Interpretation of nonelectrolyte partition coefficients between dimyristoyl lecithin and water, J. Membr. Biol. 17 (1) (1974) 121–154. doi:10.1007/BF01870176.

[43] S. J. Marrink, H. J. C. Berendsen, Simulation of water transport through a lipid membrane, J. Phys. Chem. 98 (1994) 4155–4168.

[44] H. J. C. Berendsen, S.-J. Marrink, Molecular dynamics of water transport through membranes: Water from solvent to solute, Pure Appl. Chem. 65 (1993) 2513–2520. doi:10.1351/pac199365122513.

[45] G. Parisio, M. Stocchero, A. Ferrarini, Passive membrane permeability: Beyond the standard solubility-diffusion model, J. Comp. Theory. Comput. 9 (12) (2013) 5236–5246. doi:10.1021/ct400690t.

[46] W. F. D. Bennett, D. P. Tieleman, The importance of membrane defects – lessons from simulations, Acc. Chem. Res. 47 (8) (2014) 2244–2251. doi:10.1021/ar4002729.

[47] C. Neale, C. Madill, S. Rauscher, R. Pomès, Accelerating convergence in molecular dynamics simulations of solutes in lipid membranes by conducting a random walk along the bilayer normal, J. Chem. Theory. Comput. 9 (8) (2013) 3686–3703. doi:10.1021/ct301005b.

[48] C. L. Wennberg, D. van der Spoel, J. S. Hub, Large influence of cholesterol on solute partitioning into lipid membranes, J. Am. Chem. Soc. 134 (11) (2012) 5351–5361. doi:10.1021/ja211929h.

[49] S. Riahi, C. N. Rowley, Why can hydrogen sulfide permeate cell membranes?, J. Am. Chem. Soc. 136 (43) (2014) 15111–15113. doi:10.1021/ja508063s.

[50] W. L. Jorgensen, J. Chandrasekhar, J. D. Madura, R. W. Impey, M. L. Klein, Comparison of simple potential functions for simulating liquid water, J. Chem. Phys. 79 (2) (1983) 926–935. doi:10.1063/1.445869.

[51] W. L. Jorgensen, J. D. Madura, Temperature and size dependence for monte carlo simulations of tip4p water, Mol. Phys. 56 (6) (1985) 1381–1392. doi:10.1080/00268978500103111.

[52] O. Berger, O. Edholm, F. Jähnig, Molecular dynamics simulations of a fluid bilayer of dipalmitoylphosphatidylcholine at full hydration, constant pressure, and constant temperature, Biophys. J. 72 (5) (1997) 2002–2013. doi:10.1016/S0006-3495(97)78845-3.

[53] J. B. Klauda, R. M. Venable, J. A. Freites, J. W. O'Connor, D. J. Tobias, C. Mondragon-Ramirez, I. Vorobyov, A. D. MacKerell Jr., R. W. Pastor, Update of the CHARMM all-atom additive force field for lipids: validation on six lipid types, J. Phys. Chem. B 114 (2010) 7830–7843.

[54] J. Wang, R. M. Wolf, J. W. Caldwell, P. A. Kollman, D. A. Case, Development and testing of a general amber force field, J. Comput. Chem. 25 (9) (2004) 1157–1174. doi:10.1002/jcc.20035.

[55] W. L. Jorgensen, J. Tirado-Rives, Potential energy functions for atomic-level simulations of water and organic and biomolecular systems, Proc. Natl. Acad. Sci. U.S.A. 102 (19) (2005) 6665–6670. doi:10.1073/pnas.0408037102.

[56] K. Vanommeslaeghe, E. Hatcher, C. Acharya, S. Kundu, S. Zhong, J. Shim, E. Darian, O. Guvench, P. Lopes, I. Vorobyov, A. D. Mackerell Jr., Charmm general force field: A force field for drug-like molecules compatible with the charmm all-atom additive biological force fields, J. Comput. Chem. 31 (4) (2010) 671–690. doi:10.1002/jcc.21367.

[57] G. M. Torrie, J. P. Valleau, Nonphysical sampling distributions in monte carlo free-energy estimation: Umbrella sampling, J. Comput. Phys. 23 (1977) 187–199.

[58] J. Kästner, Umbrella sampling, Wiley Interdiscip. Rev. Comput. Mol. Sci. 1 (6) (2011) 932–942. doi:10.1002/wcms.66.

[59] J. L. MacCallum, D. P. Tieleman, Computer simulation of the distribution of hexane in a lipid bilayer: spatially resolved free energy,

entropy, and enthalpy profiles, J. Am. Chem. Soc. 128 (1) (2006) 125–130. doi:10.1021/ja0535099.

[60] C. Neale, W. D. Bennett, D. P. Tieleman, R. Pomès, Statistical convergence of equilibrium properties in simulations of molecular solutes embedded in lipid bilayers, J. Chem. Theory Comput. 7 (2011) 4175–4188.

[61] S. Kumar, D. Bouzida, R. Swendsen, P. Kollman, J. Rosenberg, The Weighted Histogram Analysis Method for free-energy calculations on biomolecules. I. the method., J. Comput. Chem. 13 (1992) 1011–1021.

[62] B. Roux, The calculation of the potential of mean force using computer simulations, Comput. Phys. Commun. 91 (1–3) (1995) 275–282. doi:10.1016/0010-4655(95)00053-I.

[63] M. R. Shirts, J. D. Chodera, Statistically optimal analysis of samples from multiple equilibrium states, J. Chem. Phys. 129 (12) (2008) 124105. doi:10.1063/1.2978177.

[64] Y. Sugita, A. Kitao, Y. Okamoto, Multidimensional replica-exchange method for free-energy calculations, J. Chem. Phys. 113 (15) (2000) 6042–6051. doi:10.1063/1.1308516.

[65] S. Rauscher, C. Neale, R. Pomès, Simulated tempering distributed replica sampling, virtual replica exchange, and other generalized-ensemble methods for conformational sampling, J. Chem. Theory Comput. 5 (10) (2009) 2640–2662. doi:10.1021/ct900302n.

[66] K. Huang, A. E. García, Acceleration of lateral equilibration in mixed lipid bilayers using replica exchange with solute tempering, J. Chem. Theory Comput. 10 (10) (2014) 4264–4272. doi:10.1021/ct500305u.

[67] J. P. M. Jämbeck, A. P. Lyubartsev, Exploring the free energy landscape of solutes embedded in lipid bilayers, J. Phys. Chem. Lett. 4 (11) (2013) 1781–1787. doi:10.1021/jz4007993.

[68] S. Jo, H. Rui, J. B. Lim, J. B. Klauda, W. Im, Cholesterol flip-flop: Insights from free energy simulation studies, J. Phys. Chem. B 114 (42) (2010) 13342–13348. doi:10.1021/jp108166k.

[69] J. Comer, K. Schulten, C. Chipot, Diffusive models of membrane permeation with explicit orientational freedom, J. Chem. Theory Comput. 10 (2014) 2710–2718.

[70] G. Parisio, M. M. Sperotto, A. Ferrarini, Flip-flop of steroids in phospholipid bilayers: Effects of the chemical structure on transbilayer diffusion, J. Am. Chem. Soc. 134 (29) (2012) 12198–12208. doi:10.1021/ja304007t.

[71] A. Einstein, Investigations on the Theory of the Brownian Movement, Dover Books on Physics Series, Dover Publications, 1956.

[72] R. Kubo, The fluctuation-dissipation theorem, Reports on Progress in Physics 29 (1) (1966) 255.

[73] G. Hummer, Position-dependent diffusion coefficients and free energies from bayesian analysis of equilibrium and replica molecular dynamics simulations, New J. Phys. 7 (2005) 34.

[74] M. Orsi, W. E. Sanderson, J. W. Essex, Permeability of small molecules through a lipid bilayer: A multiscale simulation study, J. Phys. Chem. B 113 (35) (2009) 12019–12029. doi:10.1021/jp903248s.

[75] T. B. Woolf, B. Roux, Molecular dynamics simulation of the gramicidin channel in a phospholipid bilayer, Proc. Natl. Acad. Sci. USA 91 (1994) 11631–11635.

[76] S. Crouzy, T. Woolf, B. Roux, A molecular dynamics study of gating in dioxolane-linked gramicidin a channels, Biophys. J. 67 (4) (1994) 1370–1386. doi:10.1016/S0006-3495(94)80618-6.

[77] M. F. Schumaker, R. Pomès, B. Roux, A combined molecular dynamics and diffusion model of single proton conduction through gramicidin, Biophys. J. 79 (6) (2000) 2840–2857. doi:10.1016/S0006-3495(00)76522-2.

[78] M. Allen, D. Tildesley, Computer Simulation of Liquids, Oxford Science Publications, Clarendon Press, Oxford, 1989.

[79] F. Zhu, G. Hummer, Theory and simulation of ion conduction in the pentameric glic channel, J. Chem. Theory Comput. 8 (10) (2012) 3759–3768. doi:10.1021/ct2009279.

[80] H. Flyvbjerg, H. G. Petersen, Error estimates on averages of correlated data, J. Chem. Phys 91 (1) (1989) 461–466. doi:10.1063/1.457480.

[81] M. L. Mugnai, R. Elber, Extracting the diffusion tensor from molecular dynamics simulation with milestoning, J. Chem. Phys 142 (1) (2015) 014105. doi:10.1063/1.4904882.

[82] J. Comer, C. Chipot, F. D. Gonzlez-Nilo, Calculating position-dependent diffusivity in biased molecular dynamics simulations, J. Chem. Theory Comput. 9 (2) (2013) 876–882. doi:10.1021/ct300867e.

[83] S. J. Marrink, H. J. C. Berendsen, Permeation process of small molecules across lipid membranes studied by molecular dynamics simulations, J. Phys. Chem 100 (41) (1996) 16729–16738. doi:10.1021/jp952956f.

[84] I. V. Khavrutskii, A. A. Gorfe, B. Lu, J. A. McCammon, Free energy for the permeation of Na^+ and Cl^- ions and their ion-pair through a zwitterionic dimyristoyl phosphatidylcholine lipid bilayer by umbrella integration with harmonic fourier beads, J. Am. Chem. Soc. 131 (5) (2009) 1706–1716. doi:10.1021/ja8081704.

[85] L. Li, I. Vorobyov, T. W. Allen, The different interactions of lysine and arginine side chains with lipid membranes, J. Phys. Chem. B 117 (40) (2013) 11906–11920. doi:10.1021/jp405418y.

[86] J. L. MacCallum, W. D. Bennett, D. P. Tieleman, Transfer of arginine into lipid bilayers is nonadditive, Biophys. J. 101 (1) (2011) 110–117. doi:10.1016/j.bpj.2011.05.038.

[87] D. Sun, J. Forsman, C. E. Woodward, Evaluating force fields for the computational prediction of ionized arginine and lysine side-chains partitioning into lipid bilayers and octanol, J. Chem. Theory Comput. 11 (4) (2015) 1775–1791. doi:10.1021/ct501063a.

[88] I. Vorobyov, T. E. Olson, J. H. Kim, R. E. K. II, O. S. Andersen, T. W. Allen, Ion induced defect permeation of lipid membranes, Biophys. J. 106 (3) (2014) 586–597. doi:10.1016/j.bpj.2013.12.027.

[89] B. Roux, Lonely arginine seeks friendly environment, J. Gen. Physiol. 130 (2) (2007) 233–236. doi:10.1085/jgp.200709819.
URL `http://jgp.rupress.org/content/130/2/233.short`

[90] D. Bemporad, J. Essex, C. Luttmann, Permeation of small molecules through a lipid bilayer: A computer simulation study, J. Phys. Chem. B 108 (2004) 4875–4884.

[91] Y. Mao, Y. Zhang, Thermal conductivity, shear viscosity and specific heat of rigid water models, Chem. Phys. Lett. 542 (2012) 37–41. doi:10.1016/j.cplett.2012.05.044.

[92] M. Orsi, J. Michel, J. W. Essex, Coarse-grain modelling of DMPC and DOPC lipid bilayers, J. Phys. Condens. Matter 22 (15) (2010) 155106.

[93] B. W. Holland, M. D. Berry, C. G. Gray, B. Tomberli, A permeability study of O_2 and the trace amine p-tyramine through model phosphatidylcholine bilayers, PLoS ONE 10 (6) (2015) e0122468. doi:10.1371/journal.pone.0122468.

[94] D. Papahadjopoulos, M. Cowden, H. Kimelberg, Role of cholesterol in membranes effects on phospholipid-protein interactions, membrane permeability and enzymatic activity, Biochimica et Biophysica Acta (BBA) - Biomembranes 330 (1) (1973) 8–26. doi:10.1016/0005-2736(73)90280-0.

[95] L. R. D. Young, K. A. Dill, Solute partitioning into lipid bilayer membranes, Biochemistry 27 (14) (1988) 5281–5289. doi:10.1021/bi00414a050.

[96] E. C. Yan, K. B. Eisenthal, Effect of cholesterol on molecular transport of organic cations across liposome bilayers probed by second harmonic generation, Biophys. J. 79 (2) (2000) 898–903. doi:10.1016/S0006-3495(00)76345-4.

[97] P. Jedlovszky, M. Mezei, Effect of cholesterol on the properties of phospholipid membranes. 2. free energy profile of small molecules, J. Phys. Chem. B 107 (22) (2003) 5322–5332. doi:10.1021/jp021951x.

[98] J. S. Hub, F. K. Winkler, M. Merrick, B. L. de Groot, Potentials of mean force and permeabilities for carbon dioxide, ammonia, and water flux across a rhesus protein channel and lipid membranes, J. Am. Chem. Soc. 132 (38) (2010) 13251–13263. doi:10.1021/ja102133x.

[99] E. S. E. Eriksson, L. A. Eriksson, The influence of cholesterol on the properties and permeability of hypericin derivatives in lipid membranes, J. Chem. Theory. Comput. 7 (3) (2011) 560–574. doi:10.1021/ct100528u.

[100] H. Saito, W. Shinoda, Cholesterol effect on water permeability through DPPC and PSM lipid bilayers: A molecular dynamics study, J. Phys. Chem. B 115 (51) (2011) 15241–15250. doi:10.1021/jp201611p.

[101] B. B. Issack, G. H. Peslherbe, Effects of cholesterol on the thermodynamics and kinetics of passive transport of water through

lipid membranes, J. Phys. Chem. B 119 (29) (2015) 9391–9400. doi:10.1021/jp510497r.

[102] F. Zocher, D. van der Spoel, P. Pohl, J. Hub, Local partition coefficients govern solute permeability of cholesterol-containing membranes, Biophys. J. 105 (12) (2013) 2760–2770. doi:10.1016/j.bpj.2013.11.003.

[103] C. P. Moon, K. G. Fleming, Side-chain hydrophobicity scale derived from transmembrane protein folding into lipid bilayers, Proc. Natl. Acad. Sci. U.S.A. 108 (25) (2011) 10174–10177. doi:10.1073/pnas.1103979108.

[104] A. C. V. Johansson, E. Lindahl, The role of lipid composition for insertion and stabilization of amino acids in membranes, J. Chem. Phys. 130 (18) (2009) 185101. doi:10.1063/1.3129863.

[105] G. Lamoureux, B. Roux, Modeling induced polarization with classical drude oscillators: Theory and molecular dynamics simulation algorithm, J. Chem. Phys. 119 (6) (2003) 3025–3039. doi:10.1063/1.1589749.

[106] P. Lopes, B. Roux, A. MacKerell Jr., Molecular modeling and dynamics studies with explicit inclusion of electronic polarizability: theory and applications, Theor. Chem. Acc. 124 (2009) 11–28.

[107] S. Patel, C. L. Brooks III, Fluctuating charge force fields: recent developments and applications from small molecules to macromolecular biological systems, Mol. Simul. 32 (3-4) (2006) 231–249. doi:10.1080/08927020600726708.

[108] J. W. Ponder, C. Wu, P. Ren, V. S. Pande, J. D. Chodera, M. J. Schnieders, I. Haque, D. L. Mobley, D. S. Lambrecht, J. Robert A. DiStasio, M. Head-Gordon, G. N. I. Clark, M. E. Johnson, T. Head-Gordon, Current status of the AMOEBA polarizable force field, J. Phys. Chem. B 114 (8) (2010) 2549–2564. doi:10.1021/jp910674d.

[109] J. E. Davis, S. Patel, Charge equilibration force fields for lipid environments: Applications to fully hydrated DPPC bilayers and DMPC-embedded gramicidin A, J. Phys. Chem. B 113 (27) (2009) 9183–9196. doi:10.1021/jp901088g.

[110] D. Robinson, A polarizable force-field for cholesterol and sphingomyelin, J. Chem. Theory Comput. 9 (5) (2013) 2498–2503. doi:10.1021/ct400103e.

[111] E. Harder, A. D. MacKerell, Jr., B. Roux, Many-body polarization effects and the membrane dipole potential, J. Am. Chem. Soc. 131 (8) (2009) 2760–2761. doi:10.1021/ja806825g.

[112] J. Chowdhary, E. Harder, P. E. M. Lopes, L. Huang, A. D. MacKerell, Jr., B. Roux, A polarizable force field of dipalmitoylphosphatidylcholine based on the classical drude model for molecular dynamics simulations of lipids, J. Phys. Chem. B 117 (31) (2013) 9142–9160. doi:10.1021/jp402860e.

[113] B. A. Bauer, T. R. Lucas, D. J. Meninger, S. Patel, Water permeation through DMPC lipid bilayers using polarizable charge equi-

libration force fields, Chem. Phys. Lett. 508 (4-6) (2011) 289–294. doi:10.1016/j.cplett.2011.04.052.

[114] A. L. Hickey, C. N. Rowley, Benchmarking quantum chemical methods for the calculation of molecular dipole moments and polarizabilities, J. Chem. Phys. A 118 (20) (2014) 3678–3687. doi:10.1021/jp502475e.

[115] G. Lamoureux, E. Harder, I. V. Vorobyov, B. Roux, A. D. MacKerell Jr., A polarizable model of water for molecular dynamics simulations of biomolecules, Chem. Phys. Lett. 418 (13) (2006) 245–249. doi:10.1016/j.cplett.2005.10.135.

[116] J. L. F. Abascal, C. Vega, A general purpose model for the condensed phases of water: TIP4P/2005, J. Chem. Phys. 123 (23) (2005) 234505. doi:10.1063/1.2121687.

[117] D. Rozmanov, P. G. Kusalik, Transport coefficients of the TIP4P-2005 water model, J. Chem. Phys 136 (4) (2012) 044507. doi:10.1063/1.3677196.

[118] S. J. Marrink, A. H. de Vries, A. E. Mark, Coarse grained model for semiquantitative lipid simulations, J. Phys. Chem. B 108 (2) (2004) 750–760. doi:10.1021/jp036508g.

[119] S. J. Marrink, D. P. Tieleman, Perspective on the martini model, Chem. Soc. Rev. 42 (2013) 6801–6822. doi:10.1039/C3CS60093A.

[120] W. den Otter, S. Shkulipa, Intermonolayer friction and surface shear viscosity of lipid bilayer membranes, Biophys. J. 93 (2) (2007) 423–433. doi:10.1529/biophysj.107.105395.

[121] D. H. de Jong, A molecular view on the organizational complexity of proteins in membranes, Ph.D. thesis, University of Groningen (2013).

[122] A. Gauthier, B. Joós, Stretching effects on the permeability of water molecules across a lipid bilayer, J. Chem. Phys. 127 (10) (2007) 105104. doi:10.1063/1.2764079.

[123] J. Wong-Ekkabut, S. Baoukina, W. Triampo, I.-M. Tang, D. P. Tieleman, L. Monticelli, Computer simulation study of fullerene translocation through lipid membranes, Nat. Nanotechnol. 3 (6) (2008) 363–368. doi:10.1038/nnano.2008.130.

[124] H. Yuan, C. J. Jameson, S. Murad, Exploring gas permeability of lipid membranes using coarse-grained molecular dynamics, Mol. Sim. 35 (10-11) (2009) 953–961. doi:10.1080/08927020902763839.

[125] R. S. G. D'Rozario, C. L. Wee, E. J. Wallace, M. S. P. Sansom, The interaction of C60 and its derivatives with a lipid bilayer via molecular dynamics simulations, Nanotechnology 20 (11) (2009) 115102.

[126] S. O. Yesylevskyy, L. V. Schäfer, D. Sengupta, S. J. Marrink, Polarizable water model for the coarse-grained martini force field, PLoS Comput Biol 6 (6) (2010) e1000810. doi:10.1371/journal.pcbi.1000810.

[127] N. D. Winter, G. C. Schatz, Coarse-grained molecular dynamics study of permeability enhancement in DPPC bilayers by incorporation of lysolipid, J. Phys. Chem B 114 (15) (2010) 5053–5060. doi:10.1021/jp911309s.

[128] B. Song, H. Yuan, C. J. Jameson, S. Murad, Role of surface ligands in nanoparticle permeation through a model membrane: a coarse-grained molecular dynamics simulations study, Mol. Phys. 110 (18) (2012) 2181–2195. doi:10.1080/00268976.2012.668964.

[129] B. Song, H. Yuan, S. V. Pham, C. J. Jameson, S. Murad, Nanoparticle permeation induces water penetration, ion transport, and lipid flip-flop, Langmuir 28 (49) (2012) 16989–17000. doi:10.1021/la302879r.

[130] P. Gkeka, L. Sarkisov, P. Angelikopoulos, Homogeneous hydrophobic–hydrophilic surface patterns enhance permeation of nanoparticles through lipid membranes, J. Phys. Chem. Lett. 4 (11) (2013) 1907–1912. doi:10.1021/jz400679z.

[131] P. A. Oroskar, C. J. Jameson, S. Murad, Surface-functionalized nanoparticle permeation triggers lipid displacement and water and ion leakage, Langmuir 31 (3) (2015) 1074–1085. doi:10.1021/la503934c.

[132] S. M. Saparov, Y. N. Antonenko, P. Pohl, A new model of weak acid permeation through membranes revisited: Does overton still rule?, Biophys. J. 90 (11) (2006) L86 – L88. doi:10.1529/biophysj.106.084343.

[133] J. M. A. Grime, M. A. Edwards, N. C. Rudd, P. R. Unwin, Quantitative visualization of passive transport across bilayer lipid membranes, Proc. Natl. Acad. Sci. U.S.A. 105 (38) (2008) 14277–14282. doi:10.1073/pnas.0803720105.

[134] A. Missner, P. Kügler, Y. N. Antonenko, P. Pohl, Passive transport

across bilayer lipid membranes: Overton continues to rule, Proc. Natl. Acad. Sci. U.S.A. 105 (52) (2008) E123. doi:10.1073/pnas.0809606106.

[135] M. A. Wilson, A. Pohorille, Mechanism of unassisted ion transport across membrane bilayers, J. Am. Chem. Soc. 118 (28) (1996) 6580–6587. doi:10.1021/ja9540381.

[136] K. Tu, M. Tarek, M. L. Klein, D. Scharf, Effects of anesthetics on the structure of a phospholipid bilayer: Molecular dynamics investigation of halothane in the hydrated liquid crystal phase of dipalmitoylphosphatidylcholine, Biophys. J. 75 (5) (1998) 2123–2134. doi:10.1016/s0006-3495(98)77655-6.

[137] P. Jedlovszky, M. Mezei, Calculation of the free energy profile of H_2O, O_2, CO, CO_2, NO, and $CHCl_3$ in a lipid bilayer with a cavity insertion variant of the widom method, J. Am. Chem. Soc. 122 (21) (2000) 5125–5131. doi:10.1021/ja000156z.

[138] J. A. Söderhäll, A. Laaksonen, Molecular dynamics simulations of ubiquinone inside a lipid bilayer, J. Phys. Chem. B 105 (38) (2001) 9308–9315. doi:10.1021/jp011001w.

[139] D. Bas, D. Dorison-Duval, S. Moreau, P. Bruneau, C. Chipot, Rational determination of transfer free energies of small drugs across the wateroil interface, J. Med. Chem. 45 (1) (2002) 151–159. doi:10.1021/jm010289a.

[140] J. Ulander, A. Haymet, Permeation across hydrated DPPC lipid bilay-

ers: Simulation of the titrable amphiphilic drug valproic acid, Biophys. J. 85 (6) (2003) 3475–3484. doi:10.1016/s0006-3495(03)74768-7.

[141] B. G. Dzikovski, V. A. Livshits, D. Marsh, Oxygen permeation profile in lipid membranes: Comparison with transmembrane polarity profile, Biophys. J. 85 (2) (2003) 1005–1012. doi:10.1016/s0006-3495(03)74539-1.

[142] J. Milhaud, New insights into water–phospholipid model membrane interactions, Biochimica et Biophysica Acta (BBA) - Biomembranes 1663 (1-2) (2004) 19–51. doi:10.1016/j.bbamem.2004.02.003.

[143] W. Shinoda, M. Mikami, T. Baba, M. Hato, Molecular dynamics study on the effects of chain branching on the physical properties of lipid bilayers: 2. permeability, J. Phys. Chem B 108 (26) (2004) 9346–9356. doi:10.1021/jp035998+.

[144] P. Mukhopadhyay, H. J. Vogel, D. P. Tieleman, Distribution of pentachlorophenol in phospholipid bilayers: A molecular dynamics study, Biophys. J. 86 (1) (2004) 337–345. doi:10.1016/s0006-3495(04)74109-0.

[145] K. Shinoda, W. Shinoda, T. Baba, M. Mikami, Comparative molecular dynamics study of ether- and ester-linked phospholipid bilayers, J. Chem. Phys. 121 (19) (2004) 9648. doi:10.1063/1.1806791.

[146] B. Hoff, E. Strandberg, A. S. Ulrich, D. P. Tieleman, C. Posten, 2h-NMR study and molecular dynamics simulation of the location, alignment, and mobility of pyrene in POPC bilayers, Biophys. J. 88 (3) (2005) 1818–1827. doi:10.1529/biophysj.104.052399.

[147] D. Bemporad, C. Luttmann, J. Essex, Behaviour of small solutes and large drugs in a lipid bilayer from computer simulations, Biochimica et Biophysica Acta (BBA) - Biomembranes 1718 (1-2) (2005) 1–21. doi:10.1016/j.bbamem.2005.07.009.

[148] T. Sugii, S. Takagi, Y. Matsumoto, A molecular-dynamics study of lipid bilayers: Effects of the hydrocarbon chain length on permeability, J. Chem. Phys. 123 (18) (2005) 184714. doi:10.1063/1.2102900.

[149] P. Matsson, C. A. S. Bergström, N. Nagahara, S. Tavelin, U. Norinder, P. Artursson, Exploring the role of different drug transport routes in permeability screening, J. Med. Chem. 48 (2) (2005) 604–613. doi:10.1021/jm049711o.

[150] J. L. MacCallum, D. P. Tieleman, Computer simulation of the distribution of hexane in a lipid bilayer: spatially resolved free energy, entropy, and enthalpy profiles, J. Am. Chem. Soc. 128 (1) (2006) 125–130. doi:10.1021/ja0535099.

[151] K. E. Norman, H. Nymeyer, Indole localization in lipid membranes revealed by molecular simulation, Biophys. J. 91 (6) (2006) 2046–2054. doi:10.1529/biophysj.105.080275.

[152] J. C. Mathai, S. Tristram-Nagle, J. F. Nagle, M. L. Zeidel, Structural determinants of water permeability through the lipid membrane, J. Gen. Physiol. 131 (1) (2007) 69–76. doi:10.1085/jgp.200709848.

[153] J. L. MacCallum, W. F. D. Bennett, D. P. Tieleman, Distribution of

amino acids in a lipid bilayer from computer simulations, Biophys. J. 94 (9) (2008) 3393–3404. doi:10.1529/biophysj.107.112805.

[154] J. F. Nagle, J. C. Mathai, M. L. Zeidel, S. Tristram-Nagle, Theory of passive permeability through lipid bilayers, J. Gen. Phys. 131 (1) (2007) 77–85. doi:10.1085/jgp.200709849.

[155] E. R. McCarney, B. D. Armstrong, R. Kausik, S. Han, Dynamic nuclear polarization enhanced nuclear magnetic resonance and electron spin resonance studies of hydration and local water dynamics in micelle and vesicle assemblies, Langmuir 24 (18) (2008) 10062–10072. doi:10.1021/la800334k.

[156] E. Erdtman, D. J. dos Santos, L. Lögren, L. A. Eriksson, Modelling the behavior of 5-aminolevulinic acid and its alkyl esters in a lipid bilayer, Chem. Phys. Lett. 463 (1-3) (2008) 178–182. doi:10.1016/j.cplett.2008.08.021.

[157] K. Shinoda, W. Shinoda, M. Mikami, Efficient free energy calculation of water across lipid membranes, J. Comput. Chem. 29 (12) (2008) 1912–1918. doi:10.1002/jcc.20956.

[158] Y. Wang, Y. Z. Ohkubo, E. Tajkhorshid, Chapter 12 gas conduction of lipid bilayers and membrane channels, Computational Modeling of Membrane Bilayers (2008) 343–367doi:10.1016/s1063-5823(08)00012-4.

[159] P.-L. Chau, K.-M. Tu, K. Liang, S. Chan, N. Matubayasi, Free-energy change of inserting halothane into different depths of a hy-

drated DMPC bilayer, Chem. Phys. Lett. 462 (1-3) (2008) 112–115. doi:10.1016/j.cplett.2008.07.037.

[160] J. E. Davis, O. Rahaman, S. Patel, Molecular dynamics simulations of a DMPC bilayer using nonadditive interaction models, Biophys. J. 96 (2) (2009) 385–402. doi:10.1016/j.bpj.2008.09.048.

[161] C. Wei, A. Pohorille, Permeation of membranes by ribose and its diastereomers, J. Am. Chem. Soc. 131 (29) (2009) 10237–10245. doi:10.1021/ja902531k.

[162] C. Das, P. D. Olmsted, M. G. Noro, Water permeation through stratum corneum lipid bilayers from atomistic simulations, Soft Matter 5 (22) (2009) 4549. doi:10.1039/b911257j.

[163] T. J. Müller, F. Müller-Plathe, A comparison of sulfur mustard and heptane penetrating a dipalmitoylphosphatidylcholine bilayer membrane, J. Hazard Mater. 168 (1) (2009) 13–24. doi:10.1016/j.jhazmat.2009.01.140.

[164] A. A. Mamonov, V. E. Stefanov, B. F. Shchegolev, Molecular dynamics investigation of nitric oxide (ii) interaction with a model biological membrane, Biochemistry (Moscow) Supplement Series A: Membrane and Cell Biology 3 (2) (2009) 231–238. doi:10.1134/s1990747809020172.

[165] L. Monticelli, E. Salonen, P. C. Ke, I. Vattulainen, Effects of carbon nanoparticles on lipid membranes: a molecular simulation perspective, Soft Matter 5 (22) (2009) 4433. doi:10.1039/b912310e.

[166] M. Orsi, J. W. Essex, Permeability of drugs and hormones through a lipid bilayer: insights from dual-resolution molecular dynamics, Soft Matter 6 (16) (2010) 3797. doi:10.1039/c0sm00136h.

[167] M. B. Boggara, R. Krishnamoorti, Partitioning of nonsteroidal antiinflammatory drugs in lipid membranes: A molecular dynamics simulation study, Biophys. J. 98 (4) (2010) 586–595. doi:10.1016/j.bpj.2009.10.046.

[168] S. L. Fiedler, A. Violi, Simulation of nanoparticle permeation through a lipid membrane, Biophys. J. 99 (1) (2010) 144–152. doi:10.1016/j.bpj.2010.03.039.

[169] S. Mitragotri, Y. G. Anissimov, A. L. Bunge, H. F. Frasch, R. H. Guy, J. Hadgraft, G. B. Kasting, M. E. Lane, M. S. Roberts, Mathematical models of skin permeability: An overview, Int. J. Pharm. 418 (1) (2011) 115–129. doi:10.1016/j.ijpharm.2011.02.023.

[170] R. C. Van Lehn, A. Alexander-Katz, Penetration of lipid bilayers by nanoparticles with environmentally-responsive surfaces: simulations and theory, Soft Matter 7 (24) (2011) 11392. doi:10.1039/c1sm06405c.

[171] C. Wei, A. Pohorille, Permeation of nucleosides through lipid bilayers, J. Phys. Chem. B 115 (13) (2011) 3681–3688. doi:10.1021/jp112104r.

[172] M. Minozzi, G. Lattanzi, R. Benz, M. P. Costi, A. Venturelli, P. Carloni, Permeation through the cell membrane of a boron-based β-lactamase inhibitor, PLoS ONE 6 (8) (2011) e23187. doi:10.1371/journal.pone.0023187.

[173] M. Paloncov, K. Berka, M. Otyepka, Convergence of free energy profile of coumarin in lipid bilayer, J. Chem. Theory. Comput. 8 (4) (2012) 1200–1211. doi:10.1021/ct2009208.

[174] A. E. Cardenas, G. S. Jas, K. Y. DeLeon, W. A. Hegefeld, K. Kuczera, R. Elber, Unassisted transport of n -acetyl- l -tryptophanamide through membrane: Experiment and simulation of kinetics, J. Phys. Chem. B 116 (9) (2012) 2739–2750. doi:10.1021/jp2102447.

[175] Z. Ghaemi, M. Minozzi, P. Carloni, A. Laio, A novel approach to the investigation of passive molecular permeation through lipid bilayers from atomistic simulations, J. Phys. Chem. B 116 (29) (2012) 8714–8721. doi:10.1021/jp301083h.

[176] M. B. Boggara, M. Mihailescu, R. Krishnamoorti, Structural association of nonsteroidal anti-inflammatory drugs with lipid membranes, J. Am. Chem. Soc. 134 (48) (2012) 19669–19676. doi:10.1021/ja3064342.

[177] J. Lin, B. Novak, D. Moldovan, Molecular dynamics simulation study of the effect of DMSO on structural and permeation properties of DMPC lipid bilayers, J. Phys. Chem. B 116 (4) (2012) 1299–1308. doi:10.1021/jp208145b.

[178] K. Fujimoto, N. Yoshii, S. Okazaki, Free energy profiles for penetration of methane and water molecules into spherical sodium dodecyl sulfate micelles obtained using the thermodynamic integration method combined with molecular dynamics calculations, J. Chem. Phys. 136 (1) (2012) 014511. doi:10.1063/1.3671997.

[179] M. Darvas, P. N. M. Hoang, S. Picaud, M. Sega, P. Jedlovszky, Anesthetic molecules embedded in a lipid membrane: a computer simulation study, Phys. Chem. Chem. Phys. 14 (37) (2012) 12956. doi:10.1039/c2cp41581j.

[180] B. W. Holland, C. G. Gray, B. Tomberli, Calculating diffusion and permeability coefficients with the oscillating forward-reverse method, Phys. Rev. E 86 (3). doi:10.1103/physreve.86.036707.

[181] R. Notman, J. Anwar, Breaching the skin barrier insights from molecular simulation of model membranes, Advanced Drug Delivery Reviews 65 (2) (2013) 237–250. doi:10.1016/j.addr.2012.02.011.

[182] M. Paloncýová, K. Berka, M. Otyepka, Molecular insight into affinities of drugs and their metabolites to lipid bilayers, J. Phys. Chem. B 117 (8) (2013) 2403–2410. doi:10.1021/jp311802x.

[183] D. I. Kopelevich, One-dimensional potential of mean force underestimates activation barrier for transport across flexible lipid membranes, J. Chem. Phys. 139 (13) (2013) 134906. doi:10.1063/1.4823500.

[184] P. Gkeka, L. Sarkisov, P. Angelikopoulos, Homogeneous hydrophobic–hydrophilic surface patterns enhance permeation of nanoparticles through lipid membranes, J. Chem. Theory. Comput. 4 (11) (2013) 1907–1912. doi:10.1021/jz400679z.

[185] R. V. Swift, R. E. Amaro, Back to the future: Can physical models of passive membrane permeability help reduce drug candidate attrition

and move us beyond QSPR?, Chemical Biology and Drug Design 81 (1) (2012) 61–71. doi:10.1111/cbdd.12074.

[186] A. E. Cardenas, R. Elber, Computational study of peptide permeation through membrane: searching for hidden slow variables, Mol. Phys. 111 (22-23) (2013) 3565–3578. doi:10.1080/00268976.2013.842010.

[187] P. Podloucká, K. Berka, G. Fabre, M. Paloncýová, J.-L. Duroux, M. Otyepka, P. Trouillas, Lipid bilayer membrane affinity rationalizes inhibition of lipid peroxidation by a natural lignan antioxidant, J. Phys. Chem. B 117 (17) (2013) 5043–5049. doi:10.1021/jp3127829.

[188] J. M. Nitsche, G. B. Kasting, Permeability of fluid-phase phospholipid bilayers: Assessment and useful correlations for permeability screening and other applications, J. Pharm. Sci. 102 (6) (2013) 2005–2032. doi:10.1002/jps.23471.

[189] N. A. Krylov, V. M. Pentkovsky, R. G. Efremov, Nontrivial behavior of water in the vicinity and inside lipid bilayers as probed by molecular dynamics simulations, ACS Nano 7 (10) (2013) 9428–9442. doi:10.1021/nn4042392.

[190] B. C. G. Karlsson, G. D. Olsson, R. Friedman, A. M. Rosengren, H. Henschel, I. A. Nicholls, How warfarin's structural diversity influences its phospholipid bilayer membrane permeation, J. Phys. Chem. B 117 (8) (2013) 2384–2395. doi:10.1021/jp400264x.

[191] B. Qiao, M. Olvera de la Cruz, Driving force for water permeation

across lipid membranes, J. Phys. Chem. Lett. 4 (19) (2013) 3233–3237. doi:10.1021/jz401730s.

[192] T. H. F. Thake, J. R. Webb, A. Nash, J. Z. Rappoport, R. Notman, Permeation of polystyrene nanoparticles across model lipid bilayer membranes, Soft Matter 9 (43) (2013) 10265. doi:10.1039/c3sm51225h.

[193] M. Kang, S. M. Loverde, Molecular simulation of the concentration-dependent interaction of hydrophobic drugs with model cellular membranes, J. Phys. Chem. B 118 (41) (2014) 11965–11972. doi:10.1021/jp5047613.

[194] F.-Y. Bian, J.-W. Zhang, D. Wang, S.-C. Xu, Molecular dynamics simulation of the permeation of methyldopa through POPC phospholipid bilayer membrane, Acta Physico-Chimica Sinica 30 (10) (2014) 1947–1956. doi:10.3866/PKU.WHXB201408271.

[195] G. H. Peters, M. Werge, M. N. Elf-Lind, J. J. Madsen, G. F. Velardez, P. Westh, Interaction of neurotransmitters with a phospholipid bilayer: A molecular dynamics study, Chemistry and Physics of Lipids 184 (2014) 7–17. doi:10.1016/j.chemphyslip.2014.08.003.

[196] R. M. Cordeiro, Reactive oxygen species at phospholipid bilayers: Distribution, mobility and permeation, Biochimica et Biophysica Acta (BBA) - Biomembranes 1838 (1) (2014) 438–444. doi:10.1016/j.bbamem.2013.09.016.

[197] A. Khajeh, H. Modarress, The influence of cholesterol on interactions and dynamics of ibuprofen in a lipid bilayer, Biochimica et Bio-

physica Acta (BBA) - Biomembranes 1838 (10) (2014) 2431–2438. doi:10.1016/j.bbamem.2014.05.029.

[198] A. E. Cardenas, R. Shrestha, L. J. Webb, R. Elber, Membrane permeation of a peptide: It is better to be positive, J. Phys. Chem. B 119 (21) (2015) 6412–6420. doi:10.1021/acs.jpcb.5b02122.

[199] S. Jalili, M. Saeedi, Study of curcumin behavior in two different lipid bilayer models of liposomal curcumin using molecular dynamics simulation, J. Biomol. Struct. Dyn (2015) 1–14doi:10.1080/07391102.2015.1030692.

[200] L. Yang, J. T. Kindt, Simulation study of the permeability of a model lipid membrane at the fluid–solid phase transition, Langmuir 31 (7) (2015) 2187–2195. doi:10.1021/la504269t.

[201] R. Thind, D. W. O'Neill, A. Del Regno, R. Notman, Ethanol induces the formation of water-permeable defects in model bilayers of skin lipids, Chem. Commun. 51 (25) (2015) 5406–5409. doi:10.1039/c4cc08527b.

[202] M. Casalegno, G. Raos, G. Sello, Hydrophobic aggregation and collective absorption of dioxin into lipid membranes: insights from atomistic simulations, Phys. Chem. Chem. Phys. 17 (4) (2015) 2344–2348. doi:10.1039/c4cp05466k.

[203] J. C. Phillips, R. Braun, W. Wang, J. Gumbart, E. Tajkhorshid, E. Villa, C. Chipot, R. D. Skeel, L. Kalé, K. Schulten, Scalable molec-

ular dynamics with NAMD, J. Comput. Chem. 26 (16) (2005) 1781–1802. doi:10.1002/jcc.20289.

[204] J.-P. Ryckaert, G. Ciccotti, H. J. Berendsen, Numerical integration of the cartesian equations of motion of a system with constraints: molecular dynamics of n-alkanes, J. Comput. Phys. 23 (3) (1977) 327–341. doi:10.1016/0021-9991(77)90098-5.

[205] S. Kumar, J. M. Rosenberg, D. Bouzida, R. H. Swendsen, P. A. Kollman, The weighted histogram analysis method for free-energy calculations on biomolecules. i. the method, J. Comput. Chem. 13 (8) (1992) 1011–1021. doi:10.1002/jcc.540130812.